Next-to-soft-virtual resummed rapidity distribution for the Drell-Yan process to NNLO + $\overline{\text{NNLL}}$

A. H. Ajjath,[1,2,*] Pooja Mukherjee,[1,3,†] V. Ravindran,[1,‡] Aparna Sankar,[1,§] and Surabhi Tiwari[1,‖]

[1]*The Institute of Mathematical Sciences, HBNI, Taramani, Chennai 600113, India*
[2]*Laboratoire de Physique Théorique et Hautes Energies (LPTHE), UMR 7589, Sorbonne Université et CNRS, 4 place Jussieu, 75252 Paris Cedex 05, France*
[3]*Bethe Center for Theoretical Physics, Universität Bonn, D-53115, Germany*

(Received 22 February 2022; accepted 7 July 2022; published 3 August 2022)

We present the differential predictions for the rapidity distribution of a pair of leptons through the Drell-Yan (DY) process at the LHC taking into account the soft-virtual (SV) as well as next-to-soft-virtual (NSV) resummation effects in QCD perturbation theory to next-to-next-to-leading-order plus next-to-next-to-leading-logarithmic (NNLO + $\overline{\text{NNLL}}$) accuracy. We perform the resummation in two-dimensional Mellin space using our recent formalism [A. H. Ajjath *et al.*, Phys. Rev. D **103**, L111502 (2021)] by limiting ourselves to contributions only from quark-antiquark ($q\bar{q}$) initiated channels. The resummed corrections to the fixed-order results are computed through a matched formula using the minimal prescription procedure. We find that the resummation at next-to-leading-logarithmic (next-to-next-to-leading-logarithmic) level brings about 3.98% (1.24%) corrections. We also observe that the sensitivity to the renormalization scale gets improved substantially by the inclusion of NSV resummed predictions at $\overline{\text{NNLL}}$ accuracy. Further, the lack of quark gluon (qg) initiated contributions to the NSV part in the $\overline{\text{NNLL}}$ resummed predictions leaves large factorization scale dependence, indicating their importance at NSV level as we go to higher orders in perturbation theory.

DOI: 10.1103/PhysRevD.106.034005

I. INTRODUCTION

The production of a pair of leptons, known as the Drell-Yan (DY) production [1], is one of the well-studied processes at TeV colliders such as Tevatron and the LHC. This is possible due to wealth of precise theoretical predictions both in standard model (SM) and beyond SM, taking into account corrections from various sources. Being a least-contaminated process, DY production is used as a luminosity monitor [2] at the LHC. In addition, precise data on the rates allow one to fit the parton distribution functions of hadrons [3–5]. Any deviation from the precise predictions can be used to set bounds on the parameters of models of new physics.

While the DY process at leading order (LO) is purely electroweak, the radiative corrections are dominated by QCD, and it has been an active area of interest for several decades; see Refs. [6,7] for first next-to-leading-order (NLO) results in perturbative QCD for the DY process, and for invariant mass distribution of a pair of leptons at next-to-next-to-leading order (NNLO), see Refs. [8,9]. For the same observable at next-to-next-to-next-to-leading-order (N^{3}LO) level, the dominant soft-virtual (SV) contributions were obtained in Refs. [10,11] prior to the complete result [12] at N^{3}LO becoming available recently. Electroweak (EW) correction beyond LO can be found in Refs. [13,14]. In addition to invariant mass distribution, other differential distributions, namely, rapidity and transverse momentum, are known to N^{3}LO in QCD; see Refs. [15–24]. For, mixed QCD and EW corrections, see Ref. [25], and for parton showers matched with NLO QCD results, see MC@NLO [26], POWHEG [26,27] and aMC@NLO [28] frameworks.

The fixed-order predictions are improved by resumming large threshold logarithms resulting from soft gluons; see Refs. [29–35]. For the transverse momentum distribution, at small p_T, the resulting large logarithms exponentiate in the impact parameter space [36,37]. In the soft-collinear effective theory (SCET), one performs resummation in momentum space; see Ref. [38] for inclusive production and Ref. [39] for transverse momentum distribution. In the Mellin space, resummation of large logarithms of the

*aabdulhameed@lpthe.jussieu.fr
†pmukherj@uni-bonn.de
‡ravindra@imsc.res.in
§aparnas@imsc.res.in
‖surabhit@imsc.res.in

Feynman variable x_F which describes the longitudinal momentum of the final state was achieved in Ref. [30], and it was found that there were two thresholds that could be resummed to all orders; also see Ref. [40] for a different scheme. In Ref. [41], the resummation of rapidity of $W^{\pm}$ in the Mellin-Fourier space was performed following a conjecture (see Ref. [42]), and later on, it was applied for Drell-Yan production in Refs. [43,44]. A similar approach in SCET can be found in Refs. [45,46].

Following Refs. [20,21,30], in Refs. [47,48], we studied the soft gluon resummation for the rapidity distributions of Higgs boson and also of a pair of leptons produced in hadron colliders. In the threshold limit, i.e., when the scaling variables $z_1 \to 1$ and $z_2 \to 1$, the soft gluons contribute through delta functions and plus distributions in the partonic cross sections. These contributions can be resummed to all orders both in z_1, z_2 space and in N_1, N_2 space. The resummed results known to desired logarithmic accuracy can be used to predict certain highest logarithms in the fixed order; see Refs. [21,23,49]. The threshold limit denoted by ($z_1 \to 1$, $z_2 \to 1$) corresponds to ($N_1 \to \infty$, $N_2 \to \infty$) in the Mellin-Mellin (M-M) space, giving large logarithms of the form $\ln^n(N_i)$, where $n = 1, \cdots$ and $i = 1$, 2 and the resummation in M-M space resums terms of the form $\omega = a_s\beta_0 \ln(N_1N_2)$ through a process-independent function $g(\omega)$ and a process-dependent but N_i-independent function g_0. Here, $a_s = g_s^2(\mu_R^2)/16\pi^2$, with g_s being the strong coupling constant and μ_R being the renormalisation scale. The constant β_0 is the leading coefficient of the beta function in QCD.

Contrary to naive expectation, in certain inclusive [12,50,51] and differential [52] observables, one finds that the contributions from subleading threshold logarithms, called next-to-soft-virtual (NSV) terms, contribute significantly at every order in perturbation theory. They are found to be present in most of the partonic channels unlike the leading logarithms. Thanks to the availability of these fixed-order results to unprecedented accuracy, there are enormous developments in the understanding of these subleading terms. In particular, questions related to their structure to all orders are still open; see Refs. [53–65] for more details. Recently, in a series of articles [66–69], we studied a variety of inclusive observables to understand these subleading logarithms. Remarkably, we found that there exists a systematic way to sum them up to all orders in z as well as in the Mellin N spaces, exactly the way one sums up leading threshold ones. This was achieved only for the diagonal channels. One finds that resummation of both SV and NSV terms can be achieved N space. Later on, this was extended to study NSV terms present in rapidity distributions [70] of a pair of leptons in DY and a Higgs boson in gluon fusion as well as in bottom quark annihilation. For a generic case of n-colorless particles in the final state, see Ref. [71]. Like the inclusive one, these subleading logarithms can be resummed to all orders in multidimensional space (spanned by z_l or N_l) along with the leading threshold logarithms In the present paper, we discuss the phenomenological aspects of resummed NSV terms for the production of a pair of leptons at the LHC. In the subsequent sections, we briefly recapitulate the relevant theoretical results followed by a detailed study on the numerical impact of NSV contributions, and finally we conclude our findings.

II. THEORETICAL OVERVIEW

In the QCD improved parton model, the double-differential distribution of a pair of leptons in the DY process with respect to their invariant mass q^2 and rapidity y can be written as

$$\frac{d^2\sigma^q(\tau,q^2,y)}{dq^2dy} = \sigma_{\rm B}^q(x_1^0,x_2^0,q^2)\sum_{ab=q,\bar{q},g}\int_{x_1^0}^1\frac{dz_1}{z_1}\int_{x_2^0}^1\frac{dz_2}{z_2} \times f_a\left(\frac{x_1^0}{z_1},\mu_F^2\right)f_b\left(\frac{x_2^0}{z_2},\mu_F^2\right) \times \Delta_{d,ab}^q(z_1,z_2,q^2,\mu_F^2,\mu_R^2), \tag{1}$$

where $\sigma_{\rm B}^q(x_1^0,x_2^0,q^2)$ is the Born cross section. The dimensionless scaling variable τ is given by $\tau = q^2/S = x_1^0x_2^0$, where q is the momentum of the pair of leptons and $S = (p_1+p_2)^2$ is the center-of-mass energy of the incoming hadron with momenta p_i. The rapidity y of the lepton pair is given by $y = \frac{1}{2}\ln(\frac{p_2\cdot q}{p_1\cdot q}) = \frac{1}{2}\ln(\frac{x_1^0}{x_2^0})$. The parton distribution functions of incoming partons a and b are nonperturbative and are denoted by $f_a(\frac{x_1^0}{z_1},\mu_F^2)$ and $f_b(\frac{x_2^0}{z_2},\mu_F^2)$, where x_1^0/z_1 and x_2^0/z_2 are their momentum fractions, respectively, and are renormalized at the factorization scale μ_F. $\Delta_{d,ab}^q(a_s,z_1,z_2,q^2,\mu_F^2)$ are the Drell-Yan coefficient functions (CFs) obtained from the partonic subprocesses after mass factorization at the scale μ_F and are calculable order by order in QCD perturbation theory in powers of a_s. These CFs beyond leading order in perturbation theory contain distributions such as $\delta(1-z_i)$ and $[\frac{\ln^{m-1}(1-z_i)}{1-z_i}]_+$ with $m \le 2n$, n being the order of perturbation and regular functions of z_i. Distributions show up only in the diagonal CFs, called SV terms and denoted by $\Delta_{d,q}^{\rm SV}$, while the regular part, also called the hard part, is given by $\Delta_{d,ab}^{q,H}$. The leading terms in the hard part in the threshold expansion are nothing but the NSV terms. Unlike the SV terms, the NSV terms get contributions from both diagonal as well as nondiagonal channels. Each term belonging to NSV contribution contains a pair of either $\delta(1-z_i), i = 1,\ 2,$ or $\mathcal{D}_l(z_i), i = 1,2; l \ge 0$, where $\mathcal{D}_l(z_i) = [\frac{\ln^l(1-z_i)}{1-z_i}]_+$ and regular term $\log^k(1-z_j), j = 1,2; k \ge 0$. Following the work by Catani and Trentadue [30], in Refs. [20,21,23], the resummation of SV terms for the rapidity distribution to all

orders was achieved in the scaling variables z_i in z_1, z_2 space and later extended it to N_1, N_2 space in Refs. [47,48] by performing two-dimensional Mellin transformations in the large N_1, N_2 limit to obtain resummed result in the M-M space. In the Mellin N_l space, when N_l are large, the NSV terms take the form $\ln^k N_j/N_l$ with $(j,l=1,2)$, $(k=0,1\cdots)$ up to $1/N_1^\alpha/N_2^\beta, \alpha,\beta \geq 1$. In Ref. [70], restricting to diagonal channels, they were systematically resummed to all orders along with SV terms.

The diagonal CF, taking into account both SV and NSV, denoted by $\Delta_{d,q}^{\mathrm{SV+NSV}}$, was shown to exponentiate in Ref. [70] as

$$\Delta_{d,q}^{\mathrm{SV+NSV}} = \mathcal{C}\exp(\Psi_d^q(q^2,\mu_R^2,\mu_F^2,\bar{z}_1,\bar{z}_2,\epsilon))|_{\epsilon=0}, \quad (2)$$

where the symbol "$\mathcal{C}$" refers to convolution which acts on any exponential of a function $f(z)$ takes the following expansion:

$$\mathcal{C}e^{f(z)} = \delta(1-z) + \frac{1}{1!}f(z) + \frac{1}{2!}(f\otimes f)(z) + \cdots \quad (3)$$

Here, we keep only SV distributions, namely, $\delta(\bar{z}_l)\delta(\bar{z}_j)$, $\delta(\bar{z}_l)\mathcal{D}_i(z_j)$, $\mathcal{D}_i(z_l)\mathcal{D}_k(z_j)$, and NSV terms $\mathcal{D}_i(z_l)\ln^k(\bar{z}_j)$ and $\delta(\bar{z}_l)\ln^k(\bar{z}_j)$ with $(l,j=1,2)(i,k=0,1,\ldots)$ resulting from the convolutions. In (2), ϵ is the complex valued parameter in the dimensional regularization scheme. The function Ψ_d^q in the above equation has the integral representation in z space

$$\begin{aligned}\Psi_d^q = {}& \frac{\delta(\bar{z}_1)}{2}\left(\int_{\mu_F^2}^{q^2\bar{z}_2}\frac{d\lambda^2}{\lambda^2}\mathcal{P}^q(a_s(\lambda^2),\bar{z}_2) + \mathcal{Q}_d^q(a_s(q_2^2),\bar{z}_2)\right)_+ \\ & + \frac{1}{4}\left(\frac{1}{\bar{z}_1}\left\{\mathcal{P}^q(a_s(q_{12}^2),\bar{z}_2) + 2L^q(a_s(q_{12}^2),\bar{z}_2)\right.\right. \\ & \left.\left. + q^2\frac{d}{dq^2}(\mathcal{Q}_d^q(a_s(q_2^2),\bar{z}_2) + 2\varphi_{d,q}^f(a_s(q_2^2),\bar{z}_2))\right\}\right)_+ \\ & + \frac{1}{2}\delta(\bar{z}_1)\delta(\bar{z}_2)\ln(g_{d,0}^q(a_s(\mu_F^2))) + \bar{z}_1\leftrightarrow\bar{z}_2, \end{aligned} \quad (4)$$

where $\bar{z}_l = 1-z_l$, $q_l^2 = q^2(1-z_l)$, $q_{12}^2 = q^2\bar{z}_1\bar{z}_2$ and the subscript $+$ indicates standard plus distribution.

In (4), $\mathcal{P}^q(a_s,\bar{z}_l) = P^q(a_s,\bar{z}_l) - 2B^q(a_s)\delta(\bar{z}_l)$, with $P^q(a_s,\bar{z}_l)$ being the splitting function in QCD, which takes the form

$$P^q(a_s,\bar{z}_l) = 2\left(\frac{A^q(a_s)}{(\bar{z}_l)_+} + B^q(a_s)\delta(\bar{z}_l) + L^q(a_s,\bar{z}_l)\right), \quad (5)$$

with A^q and B^q being the cusp and collinear anomalous dimensions, $L^q(a_s,\bar{z}_l) \equiv C^q(a_s)\ln(\bar{z}_l) + D^q(a_s)$. The cusp ($A^q$), the collinear ($B^q$) anomalous dimensions, and the constants C^q and D^q to third order are available in Refs. [72–74]. The anomalous dimensions A^q, B^q, C^q, and D^q can also be found in the Appendix of Ref. [69]. In (5), we drop those terms which contribute to nondiagonal NSV and beyond NSV terms throughout. The function $\mathcal{Q}_d^q$ in (4) is given as

$$\mathcal{Q}_d^q(a_s,\bar{z}_l) = \frac{2}{\bar{z}_l}D_d^q(a_s) + 2\varphi_{d,q}^f(a_s,\bar{z}_l). \quad (6)$$

In the above equation, the SV coefficient D_d^q is known to third order [47] in QCD, and the NSV coefficient $\varphi_{d,q}^f$ is parametrized in the following way:

$$\begin{aligned}\varphi_{d,q}^f(a_s(\lambda^2),\bar{z}_l) &= \sum_{i=1}^{\infty}\sum_{k=0}^{\infty}\hat{a}_s^i\left(\frac{\lambda^2}{\mu^2}\right)^{i\frac{\epsilon}{2}}S_\epsilon^i\varphi_{d,q}^{(i,k)}(\epsilon)\ln^k\bar{z}_l, \\ &= \sum_{i=1}^{\infty}\sum_{k=0}^{i}a_s^i(\lambda^2)\varphi_{d,i}^{q,(k)}\ln^k\bar{z}_l. \end{aligned} \quad (7)$$

The upper limit on the sum over k is controlled by the dimensionally regularized Feynman integrals that contribute to order a_s^i. The constant $g_{d,0}^q$ in (4) results from the finite part of the virtual contributions and pure $\delta(\bar{z}_l)$ terms of real emission contributions. The NSV coefficients $\varphi_{d,i}^{q,(k)}$ in (7) are known to third order [70] and are listed below,

$$\begin{aligned}
&\varphi_{d,1}^{q,(0)} = 2C_F, \quad \varphi_{d,1}^{q,(1)} = 0,\\
&\varphi_{d,2}^{q,(0)} = C_F n_f\left(-\frac{268}{27}+\frac{8}{3}\zeta_2\right) + C_F C_A\left(\frac{1000}{27}-28\zeta_3-\frac{56}{3}\zeta_2\right) + C_F^2(-16\zeta_2),\\
&\varphi_{d,2}^{q,(1)} = C_F C_A(10) + C_F^2(-10), \quad \varphi_{d,2}^{q,(2)} = C_F^2(-4),\\
&\varphi_{d,3}^{q,(0)} = C_F n_f^2\left(\frac{10856}{729}+\frac{32}{27}\zeta_3-\frac{304}{27}\zeta_2\right) + C_F C_A n_f\left(-\frac{118984}{729}+\frac{196}{3}\zeta_3+\frac{11816}{81}\zeta_2-\frac{208}{15}\zeta_2^2\right)\\
&\quad + C_F C_A^2\left(\frac{587684}{729}+192\zeta_5-\frac{21692}{27}\zeta_3-\frac{40844}{81}\zeta_2+\frac{176}{3}\zeta_2\zeta_3+\frac{656}{15}\zeta_2^2\right) + C_F^2 n_f\left(-\frac{1144}{9}+96\zeta_3+\frac{1432}{27}\zeta_2+\frac{32}{5}\zeta_2^2\right)\\
&\quad + C_F^2 C_A\left(-\frac{5143}{27}+\frac{460}{9}\zeta_3-\frac{5548}{27}\zeta_2+\frac{1312}{15}\zeta_2^2\right) + C_F^3\left(23+48\zeta_3-\frac{32}{3}\zeta_2-\frac{448}{15}\zeta_2^2\right),
\end{aligned}$$

$$\varphi_{d,3}^{q,(1)} = C_F C_A n_f\left(-\frac{256}{9}-\frac{28}{9}\zeta_2\right)+C_F C_A^2\left(\frac{244}{9}+24\zeta_3-\frac{8}{9}\zeta_2\right)+C_F^2 n_f\left(\frac{3952}{81}-\frac{64}{9}\zeta_2\right)$$
$$+C_F^2 C_A\left(-\frac{18436}{81}+\frac{544}{3}\zeta_3+\frac{436}{9}\zeta_2\right)+C_F^3\left(-\frac{64}{3}-64\zeta_3+\frac{80}{3}\zeta_2\right).$$
$$\varphi_{d,3}^{q,(2)} = C_F C_A n_f\left(-\frac{10}{3}\right)+C_F C_A^2\left(34-\frac{10}{3}\zeta_2\right)+C_F^2 n_f\left(\frac{40}{3}\right)+C_F^2 C_A\left(-96+\frac{52}{3}\zeta_2\right)+C_F^3\left(\frac{16}{3}\right),$$
$$\varphi_{d,3}^{q,(3)} = C_F^2 n_f\left(\frac{32}{27}\right)+C_F^2 C_A\left(-\frac{176}{27}\right), \tag{8}$$

where the constants $C_A = N_c$ and $C_F = (N_c^2-1)/2N_c$ are the Casimirs of $\mathrm{SU}(N_c)$ gauge group, n_f is the number of active flavors, and ζ_i are the Riemann zeta functions.

In Ref. [70], we systematically computed the analytic expression of resummed CFs in the M-M space after performing the double Mellin transformation on Δ_d^q in (2) as

$$\Delta_{d,N_1,N_2}^q = \prod_{i=1,2}\int_0^1 dz_i z_i^{N_i-1}\Delta_d^q(z_1,z_2)$$
$$= \tilde{g}_{d,0}^q \exp(\Psi_{d,N_1,N_2}^q), \tag{9}$$

where $\tilde{g}_{d,0}^q = \sum_{i=0}^{\infty} a_s^i \tilde{g}_{d,0,i}^q$. Here, the resummed result for Ψ_{d,N_1,N_2}^q takes the form

$$\Psi_{d,N_1,N_2}^q = g_{d,1}^q(\omega)\ln N_1 + \sum_{i=0}^{\infty} a_s^i\left(\frac{1}{2}g_{d,i+2}^q(\omega)+\frac{1}{N_1}\bar{g}_{d,i+1}^q(\omega)\right)$$
$$+\frac{1}{N_1}\sum_{i=0}^{\infty} a_s^i h_{d,i}^q(\omega,N_1)+(N_1\leftrightarrow N_2), \tag{10}$$

where

$$h_{d,0}^q(\omega,N_l) = h_{d,00}^q(\omega)+h_{d,01}^q(\omega)\ln N_l,$$
$$h_{d,i}^q(\omega,N_l) = \sum_{k=0}^{i} h_{d,ik}^q(\omega)\ln^k N_l, \tag{11}$$

with $\omega = a_s\beta_0 \ln N_1 N_2$. The SV resummation coefficients, which comprises $\tilde{g}_{d,0}^q$ and $g_{d,i}^q$, are extensively discussed in Refs. [47,75,76]. The NSV coefficients $\bar{g}_{d,i}^q$ and $h_{d,ik}^q$ are listed in Appendixes A and B. Our next task is to include these resummed contributions consistently in the fixed-order predictions to understand the phenomenological relevance of the NSV resummed results in the context of rapidity distribution for the lepton pair production in the Drell-Yan process.

III. PHENOMENOLOGY

In this section, we study the impact of resummed soft virtual plus next-to-soft-virtual (SV + NSV) results for the rapidity distribution of a pair of leptons produced through Z and γ^* in the collision of two hadrons at the LHC with center-of-mass energy 13 TeV. We take $n_f = 5$ flavors, the MMHT2014(68cl) Parton distribution function (PDF) set [77] and the corresponding $a_s(M_Z)$ through the Les Houches Accord PDF (LHAPDF) [78] interface at each order in perturbation theory. For the fixed-order rapidity distribution, we use the publicly available code VRAP0.9 [16,17]. The resummed contribution is obtained from Δ_{d,N_1,N_2}^q in (9) after performing Mellin inversions, which are done using an in-house FORTRAN-based code. The resummed results are matched to the fixed-order result in order to avoid any double-counting of threshold logarithms. The matched result is given below in (13). Here, e_q is the charge of the electron. The numerical values for the various parameters are taken from the Particle Data Group 2020 [79] and are listed below,

$$M_Z = 91.1876\ \mathrm{GeV}, \qquad \Gamma_Z = 2.4952\ \mathrm{GeV},$$
$$s_w^2 = 0.22343, \qquad \alpha = 1/128, \qquad c_w^2 = 1-s_w^2,$$
$$g_e^V = -1/4+s_w^2 \quad g_u^V = 1/4-2/3s_w^2$$
$$g_d^V = -1/4+1/3s_w^2 \quad B_e^Z = 0.03363, \tag{12}$$

$$\frac{d^2\sigma^{q,\mathrm{N^nLO+\overline{N^nLL}}}}{dq^2dy} = \frac{d^2\sigma^{q,\mathrm{N^nLO}}}{dq^2dy}+\sigma_B^q\sum_{ab\in\{q,\bar{q}\}}\int_{c_1-i\infty}^{c_1+i\infty}\frac{dN_1}{2\pi i}$$
$$\times\int_{c_2-i\infty}^{c_2+i\infty}\frac{dN_2}{2\pi i}(\tau)^{-N_1-N_2}\delta_{ab}$$
$$\times f_{a,N_1}(\mu_F^2)f_{b,N_2}(\mu_F^2)$$
$$\times(\Delta_{d,N_1,N_2}^q|_{\overline{\mathrm{N^nLL}}}-\Delta_{d,N_1,N_2}^q|_{tr\,\mathrm{N^nLO}}), \tag{13}$$

where σ_B^q is given by

$$\sigma_B^q = \frac{4\pi\alpha^2}{3q^4 N}\left[e_q^2 - \frac{2q^2(q^2-M_Z^2)e_q g_e^V g_q^V}{((q^2-M_Z^2)^2+M_Z^2\Gamma_Z^2)c_w^2 s_w^2} + \frac{3q^4\Gamma_Z B_e^Z}{16\alpha M_Z((q^2-M_Z^2)^2+M_Z^2\Gamma_Z^2)c_w^2 s_w^2} \times \left(1+\left(1-\frac{8}{3}s_w^2\right)^2\right)\right]. \quad (14)$$

The first term in (13) ($d^2\sigma^{q,\mathrm{N^nLO}}/dq^2dy$) corresponds to contributions resulting from fixed-order results up to N^{n}LO. The second term, on the other hand, contains only SV and NSV logarithms but to all orders in perturbation theory. The subscript "tr" in Δ^q_{d,N_1,N_2} indicates that it is truncated at the same order as the fixed order after expanding in powers of a_s. Hence, at a given order a_s^n, the nonzero contribution from the second term starts at order a_s^{n+1} and includes SV and NSV terms from higher orders. The Mellin space PDF ($f_{i,N}$) can be evolved using QCD-PEGASUS [80]. Alternatively, we use the technique described in Refs. [30,81] to directly deal with PDFs in the z space. The contour c_i in the Mellin inversion in (13) can be chosen according to the *minimal prescription* [82] procedure. Note that the same minimal prescription procedure for the SV terms [82] will go through for the Mellin inversion of NSV terms as well. This is because the inclusion of NSV logarithms does not introduce any new Landau pole. Further, the Landau pole problem is directly related to the fact that the coupling a_s enters into the nonperturbative region, which results because of the integration of the argument of running coupling. And the position of the Landau pole is decided by the argument of a_s in the integral representation (4), which is used to resum the large SV and NSV logarithms. Since the inclusion of NSV terms does not alter the argument of a_s in (4) from the SV case, the Landau pole will remain same as that of SV resummation. In addition, as already noted in Ref. [82], there will not be any power corrections induced for the SV resummation, and this observation continues to be valid for the NSV case as well due to the minimal prescription formula in (13).

Our numerical results for the fixed order are based on NNLO computation of the CFs in which parton distribution functions are taken up to NNLO accuracy. Although the results of fixed-order rapidity distribution at N^{3}LO are presented in Ref. [24] for the Drell-Yan process, the corresponding numerical code is not publicly available; therefore, we could not include N^{3}LO results in our analysis. The resummed SV and NSV results are computed up to NNLL accuracy. To go beyond the NNLL accuracy, we need the collinear anomalous dimensions C^q and D^q to fourth order as well as the four loop NSV coefficient $\varphi^{q,4}_{d,4}$, which are currently not available. To distinguish between SV and SV + NSV resummation, all along the paper, we denote the former by N^{n}LL and the latter by $\overline{\mathrm{N^nLL}}$ for the nth-level logarithmic accuracy.

In Tables I and II, we list the resummed exponents which are required to predict the tower of SV and NSV logarithms, respectively, in Δ^q_{d,N_1,N_2} at a given logarithmic accuracy. Let us first discuss the predictions for the SV logarithms. As shown in Table I, using the first set of resummed exponents $\{\tilde{g}^q_{d.0,0}, g^q_{d,1}\}$ which constitute to the SV-LL resummation, we get to predict the leading SV logarithms of $\Delta^{q,(i)}_{d,N_1,N_2}$ to all orders in perturbation theory, i.e., $\{\ln^l N_1 \ln^k N_2\}$ with $l+k=2i(l,k\geq 0)$ at the order a_s^i for all $i>1$. Further, using the second set of resummed exponents $\{\tilde{g}^q_{d,0,1}, g^q_{d,2}\}$ along with the first set, one can predict extra the next-to-leading SV logarithms, i.e., the towers $\{\ln^l N_1 \ln^k N_2\}$ with $l+k=2i-1, 2i-2$ for $\Delta^{q,(i)}_{d,N_1,N_2}$ with $i>2$. These towers of logarithms belong to the SV-NLL resummation. In general, using the nth set $\{\tilde{g}^q_{d,0,n}, g^q_{d,n+1}\}$ in addition to the previous sets, we can predict the highest $(2n+1)$ towers of SV logarithms in N_l with $l=1,2$, which constitutes the SV-N^{n}LL resummation, at every order in a_s^i for all $i>n+1$, where $n=0,1,2\cdots$.

Next, we discuss the predictions for the NSV logarithms present in Δ^q_{d,N_1,N_2} at a given logarithmic accuracy. As presented in Table II, using the first set of resummed exponents $\{\tilde{g}^q_{d,0,0}, g^q_{d,1}, \bar{g}^q_{d,1}, h^q_{d,0}\}$ which constitute to the $\overline{\mathrm{LL}}$ resummation, we can predict the highest NSV logarithms of $\Delta^{q,(i)}_{d,N_1,N_2}$ to all orders in perturbation theory, i.e., $\{\frac{\ln^l N_1}{N_1}\ln^k N_2, \frac{\ln^l N_2}{N_2}\ln^k N_1\}$ with $l+k=2i-1$ at the order a_s^i for all $i>1$. Similarly, using the second set of resummation exponents $\{\tilde{g}^q_{d,0,1}, g^q_{d,2}, \bar{g}^q_{d,2}, h^q_{d,1}\}$ along with the first set, one can predict the next-to-highest NSV

TABLE I. The set of resummed exponents $\{\tilde{g}^q_{d,0,n}, g^q_{d,n}(\omega)\}$, which is required to predict the tower of SV logarithms in $\Delta^{q,(n)}_{d,N_1,N_2}$ at a given logarithmic accuracy in the Mellin N space. Here, $i, j \geq 0$, and $L_l^i = \ln^i N_l$ with $l=1,2$.

GIVEN	PREDICTIONS: SV logarithms					
Resummed exponents	$\Delta^{q,(2)}_{d,N_1,N_2}$	$\Delta^{q,(3)}_{d,N_1,N_2}$	$\Delta^{q,(4)}_{d,N_1,N_2}$	$\cdots$	$\Delta^{q,(n)}_{d,N_1,N_2}$	Logarithmic accuracy
$\tilde{g}^q_{d,0,0}, g^q_{d,1}$	$\{L_1^iL_2^j\}\|_{i+j=4}$	$\{L_1^iL_2^j\}\|_{i+j=6}$	$\{L_1^iL_2^j\}\|_{i+j=8}$	$\cdots$	$\{L_1^iL_2^j\}\|_{i+j=2n}$	LL
$\tilde{g}^q_{d,0,1}, g^q_{d,2}$		$\{L_1^iL_2^j\}\|_{i+j=5,4}$	$\{L_1^iL_2^j\}\|_{i+j=7,6}$	$\cdots$	$\{L_1^iL_2^j\}\|_{i+j=2n-1,2n-2}$	NLL
$\tilde{g}^q_{d,0,2}, g^q_{d,3}$			$\{L_1^iL_2^j\}\|_{i+j=5,4}$	$\cdots$	$\{L_1^iL_2^j\}\|_{i+j=2n-3,2n-4}$	NNLL

TABLE II. The set of resummed exponents $\{\tilde{g}^q_{d,0,n}, g^q_{d,n}(\omega), \bar{g}^q_{d,n}(\omega), h^q_{d,n}(\omega)\}$, which is required to predict the tower of NSV logarithms in $\Delta^{q,(n)}_{d,N_1,N_2}$ at a given logarithmic accuracy in the Mellin N space. Here, $i,\ j \geq 0$, $L^{i,j}_{N_1,2} = \frac{\ln^i N_1}{N_1}\ln^j N_2$, and $L^{i,j}_{N_2,1} = \frac{\ln^i N_2}{N_2}\ln^j N_1$.

GIVEN Resummed exponents	PREDICTIONS: NSV logarithms					Logarithmic accuracy
	$\Delta^{q,(2)}_{d,N_1,N_2}$	$\Delta^{q,(3)}_{d,N_1,N_2}$	$\Delta^{q,(4)}_{d,N_1,N_2}$	$\cdots$	$\Delta^{q,(n)}_{d,N_1,N_2}$	
$\tilde{g}^q_{d,0,0}, g^q_{d,1}, \bar{g}^q_{d,1}, h^q_{d,0}$	$\{L^{i,j}_{N_1,2}, L^{i,j}_{N_2,1}\}\vert_{i+j=3}$	$\{L^{i,j}_{N_1,2}, L^{i,j}_{N_2,1}\}\vert_{i+j=5}$	$\{L^{i,j}_{N_1,2}, L^{i,j}_{N_2,1}\}\vert_{i+j=7}$	$\cdots$	$\{L^{i,j}_{N_1,2}, L^{i,j}_{N_2,1}\}\vert_{i+j=2n-1}$	$\overline{\text{LL}}$
$\tilde{g}^q_{d,0,1}, g^q_{d,2}, \bar{g}^q_{d,2}, h^q_{d,1}$		$\{L^{i,j}_{N_1,2}, L^{i,j}_{N_2,1}\}\vert_{i+j=4}$	$\{L^{i,j}_{N_1,2}, L^{i,j}_{N_2,1}\}\vert_{i+j=6}$	$\cdots$	$\{L^{i,j}_{N_1,2}, L^{i,j}_{N_2,1}\}\vert_{i+j=2n-2}$	$\overline{\text{NLL}}$
$\tilde{g}^q_{d,0,2}, g^q_{d,3}, \bar{g}^q_{d,3}, h^q_{d,2}$			$\{L^{i,j}_{N_1,2}, L^{i,j}_{N_2,1}\}\vert_{i+j=5}$	$\cdots$	$\{L^{i,j}_{N_1,2}, L^{i,j}_{N_2,1}\}\vert_{i+j=2n-3}$	$\overline{\text{NNLL}}$

logarithms to all orders, which includes the towers $\{\frac{\ln^l N_1}{N_1}\ln^k N_2, \frac{\ln^l N_2}{N_2}\ln^k N_1\}$ with $l+k=2i-2$ for $\Delta^{q,(i)}_{d,N_1,N_2}$ with $i > 2$. These towers of logarithms contribute to the $\overline{\text{NLL}}$ resummation. In general, using the nth set $\{\tilde{g}^q_{d,0,n}, g^q_{d,n+1}, \bar{g}^q_{d,n+1}, h^q_{d,n}\}$ in addition to the previous sets, we get to predict the highest $(n+1)$ towers of NSV logarithms in N_l with $l = 1, 2$, which constitute to the $\overline{\text{N}^\text{n}\text{LL}}$ resummation, at every order in a_s^i for all $i > n+1$.

Below, we present the resummed result given in (2) at various logarithmic accuracy and discuss the resulting predictions for the NSV logarithms in (N_1, N_2) space as displayed in Table II till a_s^4 (N^{4}LO). Note that we set $\mu_R^2 = \mu_F^2 = q^2$ in the expressions of the predictions throughout. We begin with the resummed result in the $\overline{\text{LL}}$ approximation given by

$$\Delta^{q,\overline{\text{LL}}}_{d,N_1,N_2} = \tilde{g}^q_{d,0,0}\exp\left[\ln N_1 g^q_{d,1}(\omega) + \frac{1}{N_1}\left(\bar{g}^q_{d,1}(\omega) + h^q_{d,0}(\omega, N_1)\right)\right] + (N_1 \leftrightarrow N_2). \tag{15}$$

Now, we expand the above expression up to a_s^4 (N^{4}LO) and compare the predictions for leading NSV logarithms against those from fixed-order results. Note that, as can be seen from Table II, the $\overline{\text{LL}}$ resummation, which comprises only one-loop anomalous dimensions and SV + NSV coefficients from fixed-order NLO results, predicts the leading logarithms $\{\frac{\ln^l N_1}{N_1}\ln^k N_2, \frac{\ln^l N_2}{N_2}\ln^k N_1\}\vert_{l+k=3}$, $\{\frac{\ln^l N_1}{N_1}\ln^k N_2, \frac{\ln^l N_2}{N_2}\ln^k N_1\}\vert_{l+k=5}$, $\{\frac{\ln^l N_1}{N_1}\ln^k N_2, \frac{\ln^l N_2}{N_2}\ln^k N_1\}\vert_{l+k=7}$, etc., at a_s^2 (NNLO), a_s^3 (N^{3}LO), a_s^4 (N^{4}LO), and so on, respectively, as shown below. At a_s^2 (NNLO), we have

$$\Delta^{q,(2)}_{d,N_1,N_2}\vert_{\text{NSV}-\overline{\text{LL}}} = L^3_{N_1}\{4C_F^2\} + L^{2,1}_{N_1,2}\{12C_F^2\} + L^{1,2}_{N_1,2}\{12C_F^2\} + \frac{L_2^3}{N_1}\{4C_F^2\} + (N_1 \leftrightarrow N_2). \tag{16}$$

At a_s^3 (N^{3}LO), we find

$$\Delta^{q,(3)}_{d,N_1,N_2}\vert_{\text{NSV}-\overline{\text{LL}}} = L^5_{N_1}\{4C_F^3\} + L^{4,1}_{N_1,2}\{20C_F^3\} + L^{3,2}_{N_1,2}\{40C_F^3\} + L^{2,3}_{N_1,2}\{40C_F^3\} + L^{1,4}_{N_1,2}\{20C_F^3\} + \frac{L_2^5}{N_1}\{4C_F^3\} + (N_1 \leftrightarrow N_2). \tag{17}$$

The prediction at a_s^4 (N^{4}LO) is

$$\Delta^{q,(4)}_{d,N_1,N_2}\vert_{\text{NSV}-\overline{\text{LL}}} = L^7_{N_1}\left\{\frac{8}{3}C_F^4\right\} + L^{6,1}_{N_1,2}\left\{\frac{56}{3}C_F^4\right\} + L^{5,2}_{N_1,2}\{56C_F^4\} + L^{4,3}_{N_1,2}\left\{\frac{280}{3}C_F^4\right\} + L^{3,4}_{N_1,2}\left\{\frac{280}{3}C_F^4\right\} + L^{2,5}_{N_1,2}\{56C_F^4\} + L^{1,6}_{N_1}\left\{\frac{56}{3}C_F^4\right\} + \frac{L_2^7}{N_1}\left\{\frac{8}{3}C_F^4\right\} + (N_1 \leftrightarrow N_2), \tag{18}$$

where $L^{i,j}_{N_1,2} = \frac{\ln^i N_1}{N_1}\ln^j N_2$, $L^k_{N_l} = \frac{\ln^k N_l}{N_l}$ and $L^k_l = \ln N_l$ with $l = 1, 2$. Our predictions for the leading NSV logarithms are compared against the fixed-order results in Refs. [8,9,83] up to third order.

Let us now turn to the resummed result at $\overline{\text{NLL}}$ accuracy, which reads

$$\Delta^{q,\overline{\text{NLL}}}_{d,N_1,N_2} = (\tilde{g}^q_{d,0,0} + a_s\tilde{g}^q_{d,0,1})\exp\left[\ln N_1 g^q_{d,1}(\omega) + g^q_{d,2}(\omega) + \frac{1}{N_1}\left(\bar{g}^q_{d,1}(\omega) + a_s\bar{g}^q_{d,2}(\omega) + h^q_{d,0}(\omega, N_1) + a_s h^q_{d,1}(\omega, N_1)\right)\right] + (N_1 \leftrightarrow N_2). \tag{19}$$

Note that at $\overline{\text{NLL}}$ accuracy we require anomalous dimensions up to two loops and second-order SV + NSV coefficients obtained from NNLO results. After expanding the above result up to a_s^4, we obtain the predictions for the next-to-leading NSV logarithms $\{\frac{\ln^l N_1}{N_1}\ln^k N_2, \frac{\ln^l N_2}{N_2}\ln^k N_1\}|_{l+k=4}$, $\{\frac{\ln^l N_1}{N_1}\ln^k N_2, \frac{\ln^l N_2}{N_2}\ln^k N_1\}|_{l+k=6}$, etc., at a_s^3, a_s^4, and so on, respectively, and they are given by

$$\begin{aligned}\Delta^{q,(3)}_{d,N_1,N_2}|_{\text{NSV}-\overline{\text{NLL}}} &= \Delta^{q,(3)}_{d,N_1,N_2}|_{\text{NSV}-\overline{\text{LL}}} + L^4_{N_1}\left\{\frac{110}{9}C_AC_F^2 - \frac{20}{9}C_F^2n_f + (24+40\gamma_E)C_F^3\right\} + L^{3,1}_{N_1,2}\left\{\frac{440}{9}C_AC_F^2\right.\\ &\left. - \frac{80}{9}C_F^2n_f + (80+160\gamma_E)C_F^3\right\} + L^{2,2}_{N_1,2}\left\{\frac{220}{3}C_AC_F^2 - \frac{40}{3}C_F^2n_f + (88+240\gamma_E)C_F^3\right\}\\ &+ L^{1,3}_{N_1,2}\left\{\frac{440}{9}C_AC_F^2 - \frac{80}{9}C_F^2n_f + (32+160\gamma_E)C_F^3\right\} + \frac{L_2^4}{N_1}\left\{\frac{110}{9}C_AC_F^2 - \frac{20}{9}C_F^2n_f + 40\gamma_EC_F^3\right\}\\ &+ (N_1 \leftrightarrow N_2),\end{aligned} \tag{20}$$

$$\begin{aligned}\Delta^{q,(4)}_{d,N_1,N_2}|_{\text{NSV}-\overline{\text{NLL}}} &= \Delta^{q,(4)}_{d,N_1,N_2}|_{\text{NSV}-\overline{\text{LL}}} + L^6_{N_1}\left\{\frac{154}{9}C_AC_F^3 - \frac{28}{9}C_F^3n_f + \left(24+\frac{112}{3}\gamma_E\right)C_F^4\right\} + L^{5,1}_{N_1,2}\left\{\frac{308}{3}C_AC_F^3\right.\\ &\left. - \frac{56}{3}C_F^3n_f + (128+224\gamma_E)C_F^4\right\} + L^{4,2}_{N_1,2}\left\{\frac{770}{3}C_AC_F^3 - \frac{140}{3}C_F^3n_f + (272+560\gamma_E)C_F^4\right\}\\ &+ L^{3,3}_{N_1,2}\left\{\frac{3080}{9}C_AC_F^3 - \frac{560}{9}C_F^3n_f + \left(288+\frac{2240}{3}\gamma_E\right)C_F^4\right\} + L^{2,4}_{N_1,2}\left\{\frac{770}{3}C_AC_F^3 - \frac{140}{3}C_F^3n_f\right.\\ &\left. + (152+560\gamma_E)C_F^4\right\} + L^{1,5}_{N_1,2}\left\{\frac{308}{3}C_AC_F^3 - \frac{56}{3}C_F^3n_f + (32+224\gamma_E)C_F^4\right\}\\ &+ \frac{L_2^6}{N_1}\left\{\frac{154}{9}C_AC_F^3 - \frac{28}{9}C_F^3n_f + \frac{112}{3}\gamma_EC_F^4\right\} + (N_1 \leftrightarrow N_2),\end{aligned} \tag{21}$$

where γ_E is the Euler-Mascheroni constant. The above predictions for the next-to-leading NSV logarithms are in agreement with results given in Refs. [8,9,83] up to third order. Furthermore, we have compared our full third-order results for $\Delta_d^q(z_1,z_2)$ in z space (see Ref. [70] for the third-order results in z space) with the results obtained using the generalized threshold factorization approach presented in Ref. [83]. From that comparison, we have found that our third-order prediction is in complete agreement with results given in Ref. [83] for terms of the type $\mathcal{D}_i(z_l)\ln^j(\bar{z}_m)$, $i,j \geq 0, l,m = 1,2$ in the z space. However, we could not compare the remaining $\delta(\bar{z}_l)\ln^j(\bar{z}_m)$ terms in our result because they were not available in Ref. [83].

Finally, using the $\overline{\text{NNLL}}$ resummation, which further embeds the three-loop anomalous dimensions and third-order SV + NSV coefficients obtained from N^{3}LO results, we predict the next-to-next-to-leading logarithms $\{\frac{\ln^l N_1}{N_1}\ln^k N_2, \frac{\ln^l N_2}{N_2}\ln^k N_1\}|_{i+j=5}$ at a_s^4 (N^{4}LO), $\{\frac{\ln^l N_1}{N_1}\ln^k N_2, \frac{\ln^l N_2}{N_2}\ln^k N_1\}|_{i+j=7}$ at a_s^5 (N^{5}LO), and so on. The resummed expression at $\overline{\text{NNLL}}$ accuracy is given by

$$\begin{aligned}\Delta^{q,\overline{\text{NNLL}}}_{d,N_1,N_2} &= (\tilde{g}^q_{d,0,0} + a_s\tilde{g}^q_{d,0,1} + a_s^2\tilde{g}^q_{d,0,2})\exp[\ln N_1 g^q_{d,1}(\omega)\\ &+ g^q_{d,2}(\omega) + a_s g^q_{d,3}(\omega) + \frac{1}{N_1}(\bar{g}^q_{d,1}(\omega) + a_s\bar{g}^q_{d,2}(\omega)\\ &+ a_s^2\bar{g}^q_{d,3}(\omega) + h^q_{d,0}(\omega,N_1) + a_s h^q_{d,1}(\omega,N_1)\\ &+ a_s^2 h^q_{d,2}(\omega,N_1))] + (N_1 \leftrightarrow N_2).\end{aligned} \tag{22}$$

The prediction for the next-to-next-to-leading NSV logarithm at a_s^4 is provided below:

$$\begin{aligned}\Delta^{q,(4)}_{d,N_1,N_2}|_{\text{NSV}-\overline{\text{NNLL}}} &= \Delta^{q,(4)}_{d,N_1,N_2}|_{\text{NSV}-\overline{\text{NLL}}} + L^5_{N_1}\left\{\frac{968}{27}C_A^2C_F^2 - \frac{352}{27}n_fC_F^2C_A + \frac{32}{27}C_F^2n_f^2 + \left(\frac{5392}{27}+\frac{616}{3}\gamma_E - 24\zeta_2\right)C_AC_F^3\right.\\ &\left. - \left(\frac{1000}{27}+\frac{112}{3}\gamma_E\right)C_F^3n_f + (-68+272\gamma_E+224\gamma_E^2+64\zeta_2)C_F^4\right\}\end{aligned}$$

$$+L_{N_1,2}^{4,1}\left\{\frac{4840}{27}C_A^2C_F^2-\frac{1760}{27}n_fC_F^2C_A+\frac{160}{27}C_F^2n_f^2+\left(\frac{25916}{27}+\frac{3080}{3}\gamma_E-120\zeta_2\right)C_AC_F^3\right.$$
$$\left.-\left(\frac{4712}{27}+\frac{560}{3}\gamma_E\right)C_F^3n_f+(-360+1184\gamma_E+1120\gamma_E^2+320\zeta_2)C_F^4\right\}+L_{N_1,2}^{3,2}\left\{\frac{9680}{27}C_A^2C_F^2\right.$$
$$-\frac{3520}{27}n_fC_F^2C_A+\frac{320}{27}C_F^2n_f^2+\left(\frac{48952}{27}+\frac{6160}{3}\gamma_E-240\zeta_2\right)C_AC_F^3-\left(\frac{8704}{27}+\frac{1120}{3}\gamma_E\right)C_F^3n_f$$
$$\left.+(-760+1952\gamma_E+2240\gamma_E^2+640\zeta_2)C_F^4\right\}+L_{N_1,2}^{2,3}\left\{\frac{9680}{27}C_A^2C_F^2-\frac{3520}{27}n_fC_F^2C_A+\frac{320}{27}C_F^2n_f^2\right.$$
$$+\left(1664+\frac{6160}{3}\gamma_E-240\zeta_2\right)C_AC_F^3-\left(288+\frac{1120}{3}\gamma_E\right)C_F^3n_f+(-800+1472\gamma_E+2240\gamma_E^2$$
$$\left.+640\zeta_2)C_F^4\right\}+L_{N_1,2}^{1,4}\left\{\frac{4840}{27}C_A^2C_F^2-\frac{1760}{27}n_fC_F^2C_A+\frac{160}{27}C_F^2n_f^2+\left(\frac{6568}{9}+\frac{3080}{3}\gamma_E\right.\right.$$
$$\left.\left.-120\zeta_2\right)C_AC_F^3-\left(\frac{1096}{9}+\frac{560}{3}\gamma_E\right)C_F^3n_f+(-420+464\gamma_E+1120\gamma_E^2+320\zeta_2)C_F^4\right\}$$
$$+\frac{L_2^5}{N_1}\left\{\frac{968}{27}C_A^2C_F^2-\frac{352}{27}n_fC_F^2C_A+\frac{32}{27}C_F^2n_f^2+\left(\frac{356}{3}+\frac{616}{3}\gamma_E-24\zeta_2\right)C_AC_F^3\right.$$
$$\left.-\left(\frac{56}{3}+\frac{112}{3}\gamma_E\right)C_F^3n_f+(-88+32\gamma_E+224\gamma_E^2+64\zeta_2)C_F^4\right\}. \tag{23}$$

The above predictions for the NSV logarithms in rapidity distribution $\Delta_{d,N_1,N_2}^{q,(i)}$ are found to reproduce the corresponding predictions in the inclusive cross section $\Delta_N^{q,(i)}$ computed in Ref. [69] in the limit $N_1 = N_2 = N$ for $i \leq 4$.

In Ref. [69], it has been shown, in the context of DY inclusive cross section up to N^{3}LO in the Mellin N space, that, although the total contribution of NSV logarithms is smaller as compared to the SV counterpart, it is still numerically sizeable to not be neglected. Despite being formally subleading, the considerable contribution of the NSV terms is due to their large coefficients, and this trend was also observed in the case of Higgs boson production through gluon fusion [68,84]. Here, even in the case of rapidity distribution, we expect the same trend to be observed. Keeping this in mind, we ask the following questions that can shed light on the relevance of NSV terms in the context of rapidity distribution in dilepton pair production in the DY process at the LHC:

(i) In comparison to the fixed-order corrections, how much is the effect of SV + NSV resummed results on the rapidity distribution?
(ii) How sensitive is the SV + NSV resummed rapidity distribution to the choices of factorization (μ_F) and renormalization (μ_R) scales?
(iii) How do the resummed NSV terms alter the predictions of SV resummed result?

In the following sections, we address the above questions in detail. Let us begin with analyzing the impact of SV + NSV resummed results in comparison to the fixed-order results, which is the topic of the next section. We present our results for the doubly differential distribution with respect to invariant mass q and rapidity y by plotting it as a function of y for fixed values of q.

A. Fixed-order vs resummed rapidity distribution

In this section, we study the effects of SV + NSV resummation on the fixed-order predictions for rapidity distribution of dilepton pair production in the DY process for 13 TeV LHC. Through (13), we get the resummed predictions at $\overline{\text{LL}}$, $\overline{\text{NLL}}$, and $\overline{\text{NNLL}}$ matched with the corresponding fixed-order results. The numerical impact of higher-order contributions can be quantified through the K-factors defined below,

$$\text{K}(q) = \frac{\frac{d^2\sigma}{dq^2dy}(\mu_R = \mu_F = q)}{\frac{d^2\sigma^{\text{LO}}}{dq^2dy}(\mu_R = \mu_F = q)}, \tag{24}$$

where we have set renormalization (μ_R) and factorization (μ_F) scales at q.

Figure 1 shows the K factors at LO + $\overline{\text{LL}}$, NLO + $\overline{\text{NLL}}$, and NNLO + $\overline{\text{NNLL}}$ in the right panel in comparison to the corresponding fixed-order ones depicted in the left panel as a function of rapidity y at the central scale $\mu_R = \mu_F = q$, where q is fixed at M_Z.

Below, in Table III, we show the K-factor values of both fixed-order and resummed results for benchmark rapidity values at the central scale $\mu_R = \mu_F = M_Z$. We observe that there is an enhancement of 32.9% and 36.9% when we go from LO to NLO and NNLO, respectively, at the central rapidity region. Furthermore, the fixed-order values at LO,

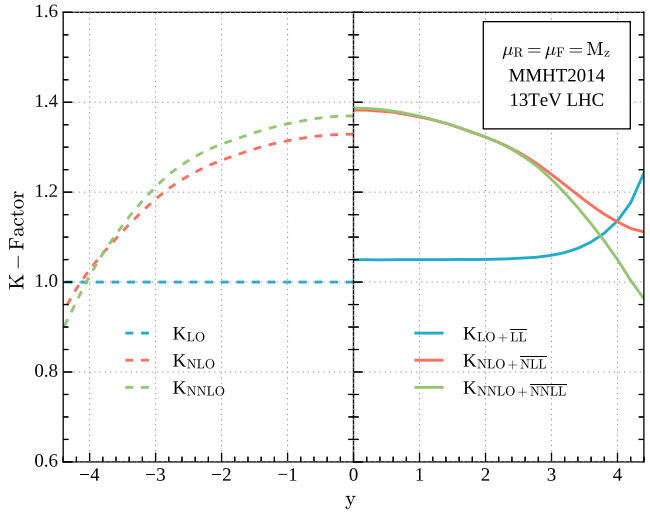

FIG. 1. The K-factor values for resummed results (right panel) in comparison to the fixed-order ones (left panel) till NNLO + $\overline{\text{NNLL}}$ level as a function of rapidity (y) at the central scale $\mu_R = \mu_F = M_Z$.

NLO, and NNLO get incremented by the inclusion of SV + NSV resummed predictions at $\overline{\text{LL}}$, $\overline{\text{NLL}}$, and $\overline{\text{NNLL}}$ by 4.9%, 3.98%, and 1.24%, respectively, around the central rapidity region. This can be seen from the right panel of Fig. 1, where the resummed curves are found to lie above their respective fixed-order ones, implying the enhancement resulting from the resummed corrections. It should be noted that the K-factor curves of the resummed results at NLO + $\overline{\text{NLL}}$ and NNLO + $\overline{\text{NNLL}}$ overlap for a wide range of rapidity values, which was not observed for the case of fixed-order predictions. This indicates that the perturbative convergence is improved among the resummed results, thereby leading to the reliability of perturbative predictions by the inclusion of resummed corrections. We also notice that the K-factor values are closer for NNLO and NNLO + $\overline{\text{NNLL}}$ as compared to NLO and NLO + $\overline{\text{NLL}}$ over the full rapidity region. This suggests that the resummed contributions to the fixed-order rapidity distribution decrease as we go to higher orders in perturbation theory.

From the above analysis of K factors, we have observed that the resummed predictions not only bring in considerable enhancement in the fixed-order results but also improve the perturbative convergence till NNLO + $\overline{\text{NNLL}}$ accuracy. However, both fixed-order and resummed predictions suffer from the presence of unphysical scales, namely, the renormalization μ_R and the factorization μ_F scales. Therefore, a careful study of perturbative uncertainties of these predictions is needed by studying their sensitivity to the choices of μ_F and μ_R scales, which will be discussed in the following subsection.

TABLE III. K-factor values of fixed-order and resummed results at the central scale $\mu_R = \mu_F = M_Z$.

y	$K_{LO+\overline{LL}}$	K_{NLO}	$K_{NLO+\overline{NLL}}$	K_{NNLO}	$K_{NNLO+\overline{NNLL}}$
0	1.049	1.329	1.382	1.369	1.386
0.8	1.05	1.319	1.372	1.358	1.374
1.6	1.05	1.291	1.343	1.327	1.343
2.4	1.502	1.245	1.296	1.279	1.295

1. Seven-point scale uncertainties of the resummed results

The uncertainty associated with the choice of renormalization μ_R and the factorization μ_F scales due to the truncation of the perturbative series can be assessed using the standard canonical seven-point variation, where $\mu = \{\mu_F, \mu_R\}$ is varied in the range $\frac{1}{2} \leq \frac{\mu}{q} \leq 2$, keeping the ratio μ_R/μ_F not larger than 2 and smaller than 1/2. In Fig. 2, we compare the seven-point scale uncertainties of the SV + NSV resummed results (right panel) against fixed-order ones (left panel) around the central scale choice $(\mu_R, \mu_F) = (M_Z, M_Z)$ for 13 Tev LHC at various perturbative orders. Here, we find that the central scale lines of resummed predictions are shifted up with respect to that of corresponding fixed-order results. This indeed suggests that there is a systematic enhancement in the rapidity distribution when we add the resummed corrections to the fixed-order results as shown in Table IV. This was also observed from the analysis of K-factor values given earlier. However, we notice that the uncertainty bands of the resummed predictions are wider than that of the corresponding fixed-order ones over the entire rapidity range at every order of perturbation. Nevertheless, the uncertainty band decreases as we go to higher logarithmic accuracy from LO + $\overline{\text{LL}}$ to NNLO + $\overline{\text{NNLL}}$. In addition, the error band of NNLO + $\overline{\text{NNLL}}$ is fully contained within the band of NLO + $\overline{\text{NLL}}$ over most of the rapidity region, unlike the fixed-order case.

In Table IV, we present both fixed order and resummed predictions at various perturbative orders along with their asymmetric errors resulting from seven-point scale variation for benchmark rapidity values. Here, we notice an increment of 31.7% while going from LO + $\overline{\text{LL}}$ to NLO + $\overline{\text{NLL}}$ accuracy, which further improves by 0.3% at NNLO + $\overline{\text{NNLL}}$ for $y = 0$. Besides this, the scale uncertainty gets reduced significantly while going from LO + $\overline{\text{LL}}$ to NNLO + $\overline{\text{NNLL}}$ over the full range of rapidity. For instance, the uncertainty ranges between $(-16.19\%, +15.36\%)$ for LO + $\overline{\text{LL}}$, $(-7.50\%, +7.06\%)$ for NLO + $\overline{\text{NLL}}$, and $(-2.18\%, +3.30\%)$ at NNLO + $\overline{\text{NNLL}}$ for the central rapidity region. However, there is no improvement in the scale uncertainty of the resummed corrections when we compare it against the fixed-order counterpart. This can be explained due to following possibilities:

(i) The resummed logarithms are not dominant in this region to show their numerical relevance.
(ii) The lack of NSV resummed corrections from off-diagonal channels can give rise to large scale uncertainties in the resummed predictions.

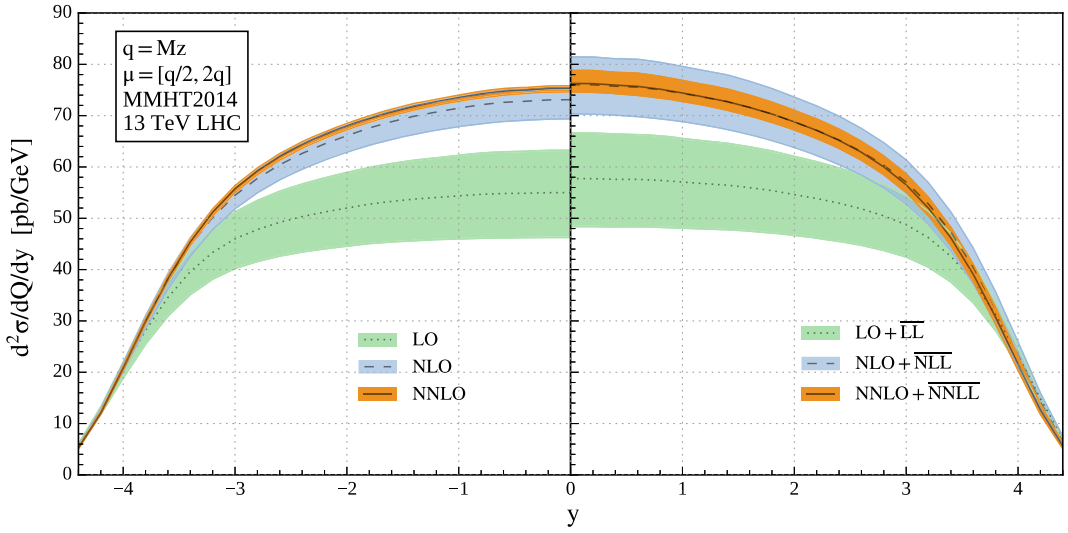

FIG. 2. Seven-point scale variation of the resummed result against fixed order around the central scale choice $(\mu_R, \mu_F) = (M_Z, M_Z)$ for 13 Tev LHC. The dotted, dashed, and solid lines refer to the corresponding central scale values at each order.

Recall that the resummation is inevitable to cure the perturbative series, which suffers from certain large logarithmic terms at every order, in the kinematic threshold region, where the invariant mass q approaches the hadronic center-of-mass energy, which is 13 TeV in our case. Therefore, to see the impact of the resummed contributions, we need to extend our analysis to the higher invariant mass region, which is of the order of TeV. We will discuss the off-diagonal channel contribution later in detail toward the end of this section. Now, we move on to the analysis of the seven-point scale uncertainty of the SV + NSV resummed predictions in comparison to the fixed-order results for high invariant mass $q = 2$ TeV.

From the earlier discussions on the seven-point scale uncertainty for $q = M_Z$, we found that the uncertainty bands of resummed predictions were wider than that of fixed order at every order of perturbation. Nevertheless, the widths of uncertainty bands were found to decrease as we moved from LO + $\overline{\text{LL}}$ to NNLO + $\overline{\text{NNLL}}$ accuracy. In addition, we also observed an appreciable amount of increment in the rapidity distribution by the inclusion of SV + NSV resummed effects. Now, here in Fig. 3, we show the seven-point scale variation of the rapidity distribution for $q = 2$ TeV. The fixed-order results are depicted in the left panel up to NNLO accuracy, and resummed predictions are given in the right panel up to NNLO + $\overline{\text{NNLL}}$ accuracy. In general, we note that the width of uncertainty bands corresponding to both fixed order as well as resummed predictions are significantly reduced as compared to the uncertainty bands for $q = M_Z$. Interestingly, the NLO + $\overline{\text{NLL}}$ uncertainty band is better as compared to NLO fixed-order band over the entire rapidity region. Also, the NNLO uncertainty gets improved by the inclusion of resummed $\overline{\text{NNLL}}$ corrections around the central rapidity region. This indicates the relevance of resummed contributions at this invariant mass region. This was not observed for the case of $q = M_Z$ where the resummed contributions were not prominent.

In Table V, we quote the central scale values of both fixed-order and resummed rapidity distributions at $q = 2$ TeV along with the seven-point scale uncertainties for benchmark rapidity values. Here, we observe that the percentage uncertainties of fixed order as well as resummed results get reduced substantially at each perturbative order when we compare them against the values given in Table IV. For instance, the uncertainty at NNLO + $\overline{\text{NNLL}}$ is reduced from $(-2.18\%, +3.3\%)$ to $(-0.31\%, +0.53\%)$ as we go from $q = M_Z$ to $q = 2$ TeV around the central rapidity region.

TABLE IV. Values of resummed rapidity distribution at various orders in comparison to the fixed-order results in pb/GeV at the central scale $\mu_R = \mu_F = M_Z$ for 13 TeV LHC.

y	LO	NLO	NNLO	LO + $\overline{\text{LL}}$	NLO + $\overline{\text{NLL}}$	NNLO + $\overline{\text{NNLL}}$
0	$55.008^{+14.99\%}_{-15.88\%}$	$73.107^{+2.951\%}_{-5.098\%}$	$75.342^{+0.6439\%}_{-0.9501\%}$	$57.730^{+15.36\%}_{-16.19\%}$	$76.049^{+7.064\%}_{-7.502\%}$	$76.283^{+3.301\%}_{-2.178\%}$
0.8	$54.674^{+14.68\%}_{-15.59\%}$	$72.137^{+3.010\%}_{-5.083\%}$	$74.237^{+0.6864\%}_{-1.011\%}$	$57.392^{+15.05\%}_{-15.91\%}$	$75.044^{+7.098\%}_{-7.482\%}$	$75.159^{+3.322\%}_{-2.233\%}$
1.6	$53.293^{+13.83\%}_{-14.80\%}$	$68.825^{+3.075\%}_{-4.988\%}$	$70.735^{+0.7423\%}_{-1.071\%}$	$55.972^{+14.19\%}_{-15.11\%}$	$71.607^{+7.078\%}_{-7.370\%}$	$71.600^{+3.311\%}_{-2.278\%}$
2.4	$50.327^{+12.63\%}_{-13.71\%}$	$62.642^{+3.154\%}_{-4.866\%}$	$64.392^{+0.8200\%}_{-1.172\%}$	$52.944^{+12.98\%}_{-14.02\%}$	$65.238^{+7.092\%}_{-7.251\%}$	$65.182^{+3.323\%}_{-2.370\%}$

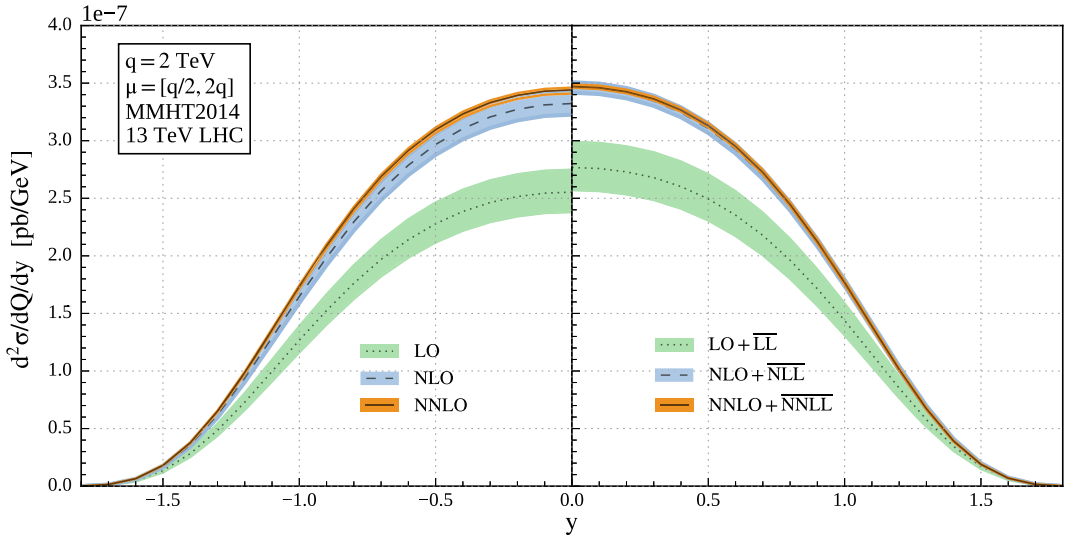

FIG. 3. Seven-point scale variation of the resummed result against fixed order around the central scale choice $(\mu_R, \mu_F) = (2, 2)$ TeV for 13 Tev LHC. The dotted, dashed, and solid lines refer to the corresponding central scale values at each order.

In addition, the uncertainty at NNLO + $\overline{\text{NNLL}}$ is evidently small as compared to the uncertainty of $(-0.89\%, +0.60\%)$ at NNLO for $y = 0$. Similarly, the uncertainty at NLO is $(-2.93\%, +2.84\%)$, which comes down to $(-1.25\%, +1.39\%)$ at NLO + $\overline{\text{NLL}}$ for the same value of y. As for the case of $q = M_z$, there is a systematic reduction in the uncertainties while going from LO + $\overline{\text{LL}}$ to NNLO + $\overline{\text{NNLL}}$ over the entire rapidity region, which can be seen from Table V. We also find that the resummed contribution at $\overline{\text{NNLL}}$ brings in 0.86% correction to NNLO, whereas it was 1.24% for the case of $q = M_Z$. This suggests that the correction resulting from resummation at $\overline{\text{NNLL}}$ accuracy decreases as we go to higher q values, leading to better reliability of resummed results.

To summarize, we found that the uncertainties of the rapidity distribution decrease by the inclusion of the resummed corrections at $q = 2$ TeV over the full rapidity region. Furthermore, the reliability of the perturbative results due to resummed corrections is improved at this invariant mass value. Thus, it can be inferred that the relevance of resummation effects becomes evidently visible while going from $q = M_z$ to $q = 2$ TeV. To understand these observations in a better way, we now turn to study the effect of each scale individually on the SV + NSV resummed result.

2. Uncertainties of the resummed results with respect to μ_R and μ_F

In the following, we examine the effect of μ_R and μ_F scales individually on the resummed result. We begin with plotting the dependence of the rapidity distribution on μ_F as a function of the rapidity y while fixing the scale μ_R at the invariant mass q, for $q = 2$ TeV as shown in Fig. 4. The bands are obtained by varying the scale μ_F by a factor of 2 up and down around the central scale $\mu_R = \mu_F = 2$ TeV. Here, the resummed band depicted in the right panel at NNLO + $\overline{\text{NNLL}}$ looks similar to that of the seven-point variation band shown in Fig. 3 (right panel). This indicates that the contribution to the width of NNLO + $\overline{\text{NNLL}}$ band in Fig. 3 mainly comes from the uncertainties arising from variations in the μ_F scale. Note that the uncertainties at NNLO + $\overline{\text{NNLL}}$ arising from μ_F and seven-point variation are identical, and they lie between $(-0.31\%, +0.53\%)$ for $y = 0$. Moreover, the μ_F scale uncertainties decrease as we go to higher logarithmic accuracy in the resummed results.

Now, we move on to compare the μ_F scale uncertainty of the resummed predictions with respect to the fixed-order results. We observe that the μ_F scale uncertainty of NLO gets improved by the inclusion of $\overline{\text{NLL}}$ resummed

TABLE V. Values of resummed rapidity distribution at various orders in comparison to the fixed-order results in 10^{-7} pb/GeV at the central scale $\mu_R = \mu_F = 2$ TeV for 13 TeV LHC.

y	LO	NLO	NNLO	LO + $\overline{\text{LL}}$	NLO + $\overline{\text{NLL}}$	NNLO + $\overline{\text{NNLL}}$
0	$2.554^{+7.627\%}_{-6.783\%}$	$3.323^{+2.836\%}_{-2.928\%}$	$3.440^{+0.597\%}_{-0.889\%}$	$2.767^{+8.026\%}_{-7.098\%}$	$3.460^{+1.395\%}_{-1.253\%}$	$3.470^{+0.533\%}_{-0.312\%}$
0.4	$2.385^{+7.914\%}_{-7.011\%}$	$3.105^{+2.881\%}_{-2.998\%}$	$3.233^{+0.600\%}_{-0.919\%}$	$2.601^{+8.360\%}_{-7.363\%}$	$3.244^{+1.408\%}_{-1.268\%}$	$3.266^{+0.596\%}_{-0.397\%}$
0.8	$1.762^{+8.836\%}_{-7.720\%}$	$2.295^{+3.079\%}_{-3.290\%}$	$2.409^{+0.647\%}_{-1.033\%}$	$1.962^{+9.438\%}_{-8.185\%}$	$2.426^{+1.563\%}_{-1.322\%}$	$2.446^{+0.7901\%}_{-0.653\%}$
1.2	$0.729^{+10.72\%}_{-9.208\%}$	$0.938^{+3.655\%}_{-3.914\%}$	$0.986^{+0.788\%}_{-1.266\%}$	$0.851^{+11.70\%}_{-9.918\%}$	$1.019^{+2.368\%}_{-1.458\%}$	$1.013^{+1.380\%}_{-1.206\%}$

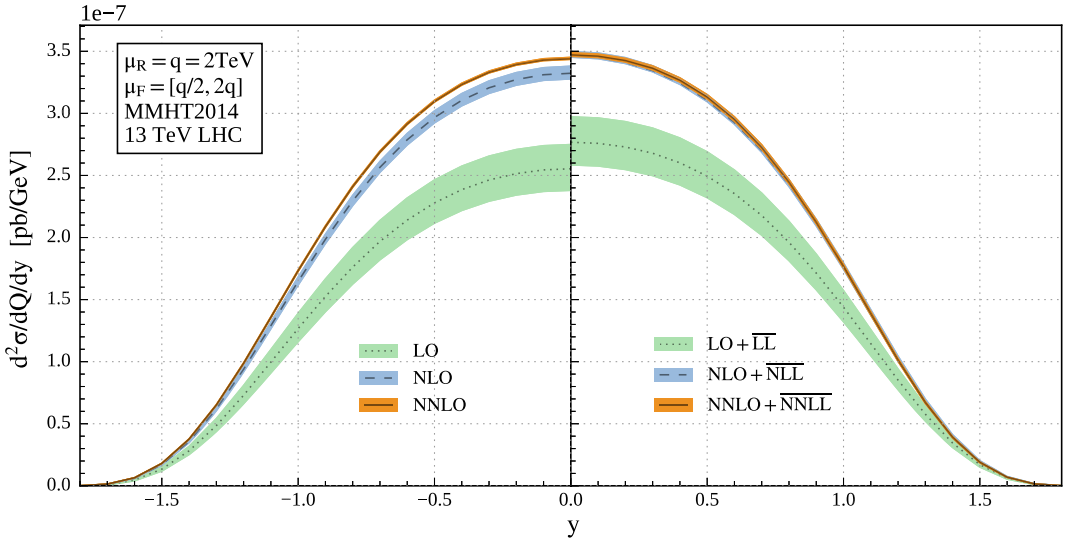

FIG. 4. μ_F scale variation of the resummed results against the fixed order with the scale μ_R held fixed at 2 for 13 TeV LHC. The dotted, dashed, and solid lines refer to the corresponding central scale values at each order.

predictions, whereas the NNLO band increases when the $\overline{\text{NNLL}}$ corrections are added. Let us try to understand why the SV + NSV resummed result at NNLO + $\overline{\text{NNLL}}$ is more sensitive to the μ_F scale variation as compared to fixed-order NNLO result. As mentioned earlier, we perform the resummation of SV distributions and NSV logarithms present in the diagonal partonic channel. Unlike the SV distributions that get contribution only from the diagonal quark-antiquark ($q\bar{q}$) initiated channel, the NSV terms can originate from off-diagonal channels like quark-gluon (qg), gluon-gluon (gg), etc., as well. Under the μ_F scale variation, these various partonic channels get mixed due to the Dokshitzer—Gribov—Lipatov—Altarelli—Parisi evolution of the PDFs. Hence, it becomes essential to keep all the contributing partonic channels at a particular perturbative order as there can be compensations among those channels, thereby reducing the scale uncertainty at that order. The fixed-order results used for our numerical analysis contain all the partonic channels, while the resummed contributions are only from $q\bar{q}$ initiated channels. Thus, the scale dependence of the fixed-order result is expected to go down in comparison to the corresponding resummed prediction.

However, as mentioned above, the inclusion of resummed corrections at $\overline{\text{NLL}}$ accuracy improves the NLO error band. This suggests that the contribution of qg channel is not prominent at NLO. We find that the one-loop correction from the $q\bar{q}$ channel is 23.6%, while the correction from the qg channel is only −2.5% of the NLO rapidity distribution at the central rapidity value. Therefore, there is an improvement in the μ_F scale uncertainty when we sum up the collinear logarithms resulting from the dominant $q\bar{q}$ channel at $\overline{\text{NLL}}$. On the other hand, at NNLO level, the a_s^2 corrections from $q\bar{q}$ and qg channels are 4.5% and −1.25%, respectively, to the NNLO rapidity distribution. As a result, the magnitude of the NNLO result is determined by a significant cancellation between $q\bar{q}$ and qg channels, which was not the case for NLO. Now, because of the unavailability of the qg resummed collinear logarithms in our analysis, the aforementioned cancellation at NNLO + $\overline{\text{NNLL}}$ is not balanced. Thus, the μ_F variation band of resummed prediction at NNLO + $\overline{\text{NNLL}}$ in Fig. 4 displays that the qg resummation is required to improve the results.

Next, we try to understand the behavior of resummed rapidity distribution in comparison to the fixed-order counterpart under μ_R scale variation. Figure 5 shows the dependence of the rapidity distribution on μ_R keeping μ_F fixed at 2 TeV. The bands are obtained by varying the scale μ_R by a factor of 2 up and down around the central scale $\mu_R = \mu_F = 2$ TeV. Here, the LO rapidity distribution, being independent of the scale μ_R, does not have a band associated with it. On the other hand, there is a band when we add the resummed corrections at $\overline{\text{LL}}$ accuracy to the LO rapidity distribution. This is because the resummed corrections at $\overline{\text{LL}}$ capture the leading logarithmic contributions from all orders in perturbation theory, thereby giving rise to μ_R scale uncertainty. Moreover, the inclusion of resummed corrections at both $\overline{\text{NLL}}$ and $\overline{\text{NNLL}}$ improves the μ_R scale uncertainties of NLO and NNLO, respectively. This is in contrast to the case of μ_F scale variation discussed earlier. Although the improvement is minuscule at NLO, it is substantial at NNLO due to NNLO + $\overline{\text{NNLL}}$, which is indeed the highlight of this plot here as compared to μ_F scale variations shown in Fig. 4. For instance, the μ_R scale uncertainty at NNLO is reduced from $(-0.56\%, +0.5\%)$ to $((-0.16\%, 0\%)$ for $y = 0$ by the inclusion of $\overline{\text{NNLL}}$. As we know, each partonic channel is invariant under μ_R scale

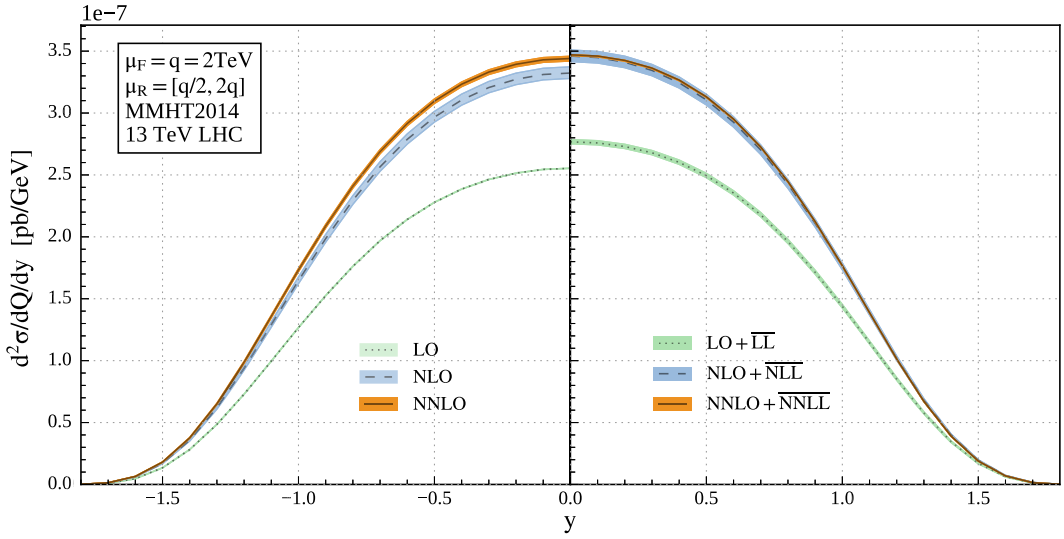

FIG. 5. μ_R scale variation of the resummed results against the fixed order with the scale μ_F held fixed at 2 for 13 TeV LHC. The dotted, dashed, and solid lines refer to the corresponding central scale values at each order.

variation when taken to all orders. Hence, there is an improvement when we include more higher-order corrections within a channel, which is $q\bar{q}$ in this case, by keeping the scale μ_F fixed.

In conclusion, we observed that the uncertainties due to both μ_F and μ_R scales decrease as we go to higher logarithmic accuracy. As far as the μ_F scale variation is concerned, the resummation of collinear logarithms resulting from the qg channel also plays an important role. We notice that having the qg resummed contribution is more significant at NNLO level than at NLO due to relatively larger contribution from qg channel at NNLO. As a result, the seven-point scale uncertainty of the SV + NSV resummed predictions at NNLO + $\overline{\text{NNLL}}$ is mostly driven by the μ_F scale variation. Note that the inclusion of SV + NSV resummed predictions reduces the μ_R scale sensitivity remarkably at NNLO + $\overline{\text{NNLL}}$ accuracy. So far, we have discussed the effects of resummation on the fixed-order results, taking into account SV distributions and NSV logarithms together in the analysis. Now, let us turn to understand which part of the SV + NSV resummation, i.e., whether it is the resummation of the distributions or of the NSV logarithms, plays the main role in any kind of improvement observed so far.

B. SV vs SV + NSV resummed results

In the previous section, we have studied the effects of SV + NSV resummation on the fixed-order rapidity distribution in detail. We observed that there is a considerable amount of enhancement in the rapidity distribution by the inclusion of SV + NSV resummed predictions and more importantly the μ_R scale uncertainty gets reduced substantially at NNLO + $\overline{\text{NNLL}}$ accuracy. On the other hand, the μ_F scale uncertainty shows improvement at NLO + $\overline{\text{NLL}}$ for higher values of q but not at NNLO + $\overline{\text{NNLL}}$. In the following, we perform an analysis on the inclusion of resummed NSV logarithms by comparing it with the SV resummed results.

We begin with the analysis of K-factor values for SV + NSV resummed results in comparison to the SV counterpart till NNLO + $\overline{\text{NNLL}}$ level at the central scale $\mu_R = \mu_F = q$ for $q = M_Z$. In Table (VI), we compare the K-factor values of SV and SV + NSV resummed predictions at various orders for benchmark rapidity values. We find that there is an increment of 3.15%, 2.75%, and 0.625% in the rapidity distribution when going from LL to $\overline{\text{LL}}$, NLL to $\overline{\text{NLL}}$, and NNLL to $\overline{\text{NNLL}}$, respectively, at the central rapidity region. Figure 6 demonstrates this trend for a wider range of rapidity values. In addition, the K-factor curves of

TABLE VI. The K-factor values for SV + NSV resummed results in comparison to the SV results till NNLO + $\overline{\text{NNLL}}$ level at the central scale $\mu_R = \mu_F = M_Z$.

y	$K_{\text{LO+LL}}$	$K_{\text{LO+}\overline{\text{LL}}}$	$K_{\text{NLO+NLL}}$	$K_{\text{NLO+}\overline{\text{NLL}}}$	$K_{\text{NNLO+NNLL}}$	$K_{\text{NNLO+}\overline{\text{NNLL}}}$
0	1.017	1.049	1.345	1.382	1.374	1.386
0.8	1.017	1.05	1.336	1.372	1.362	1.374
1.6	1.017	1.05	1.307	1.343	1.332	1.343
2.4	1.016	1.05	1.260	1.296	1.283	1.295

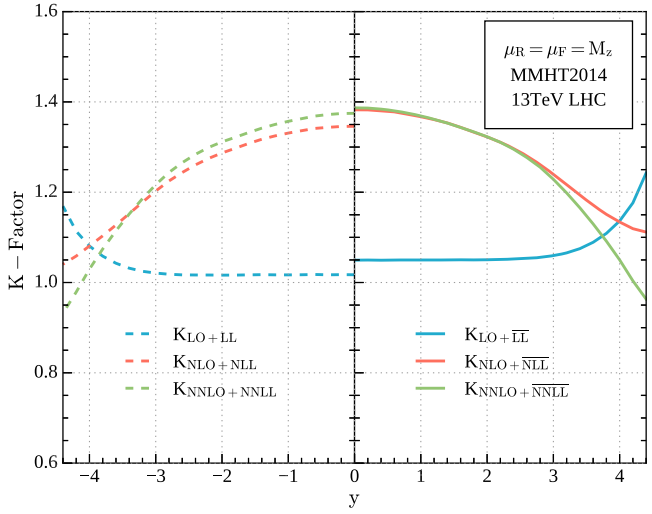

FIG. 6. The K-factor values for SV + NSV resummed results in comparison to the SV ones till NNLO + $\overline{\text{NNLL}}$ level at the central scale $\mu_R = \mu_F = M_Z$.

$\overline{\text{NLL}}$ and $\overline{\text{NNLL}}$ almost overlap with each other for a wide range of rapidity values, which is not observed for the case of NLL and NNLL curves. This suggests that there is better perturbative convergence when the NSV logarithms are taken into account.

We now turn to study the scale uncertainties arising from SV + NSV resmmation in comparison to the SV resummation. We first analyze the behavior of both SV and SV + NSV resummed rapidity distributions as a function of y under the seven-point scale variation as depicted in Fig. 7 for $q = 2$ TeV. We observe that inclusion of SV as well as SV + NSV resummed corrections reduces the uncertainty of fixed-order results at both NLO and NNLO accuracy. This reduction in the uncertainty is prominent for lower rapidity values $|y| \leq 0.5$ as shown in the insets in Fig. 7. As can be seen from the Table VII, the uncertainty at NLO + NLL is comparable to that of NLO + $\overline{\text{NLL}}$ around the central rapidity region. However, the uncertainty at NNLO + NNLL gets worse when we add the resummed NSV contributions at that accuracy. For instance, the uncertainty at NNLO + NNLL lies in the range $(-0.34\%, +0.23\%)$, whereas it is increased to $(-0.31\%, +0.53\%)$ at NNLO + $\overline{\text{NNLL}}$ for $y = 0$. This hint toward our earlier findings in the previous section that the sensitivity of the SV + NSV resummed results to the unphysical scales increases due to the lack of resummed NSV predictions from off-diagonal qg channel. Next, we move on to compare the SV and SV + NSV resummed predictions under the variation of each of these scales separately.

We first consider the behavior of both SV and SV + NSV resummed rapidity distributions as a function of y under the μ_F scale variation with the scale μ_R fixed at $q = 2$ TeV as depicted in Fig. 8. In general, the bands corresponding to SV + NSV resummed predictions are wider than that of SV predictions over the entire rapidity region. We also find that the width of the bands corresponding to fixed-order rapidity distributions gets reduced with the inclusion of both SV (NLL) and SV + NSV ($\overline{\text{NLL}}$) resummed corrections at NLO. For instance, the uncertainty is $(-1.36\%, +1.7\%)$ at NLO, whereas it is reduced to $(-0\%, 0.46\%)$ and $(-0.2\%, +1.07\%)$ at NLO + NLL and NLO + $\overline{\text{NLL}}$, respectively, for the central rapidity value. This can be associated with the earlier observation of $q\bar{q}$ and qg contributions at NLO. We have already seen that $q\bar{q}$ is the dominating channel at NLO, and hence the uncertainty is expected to get better as we include the resummed corrections coming from that channel. On the other hand, though the uncertainty at NNLO gets improved by the

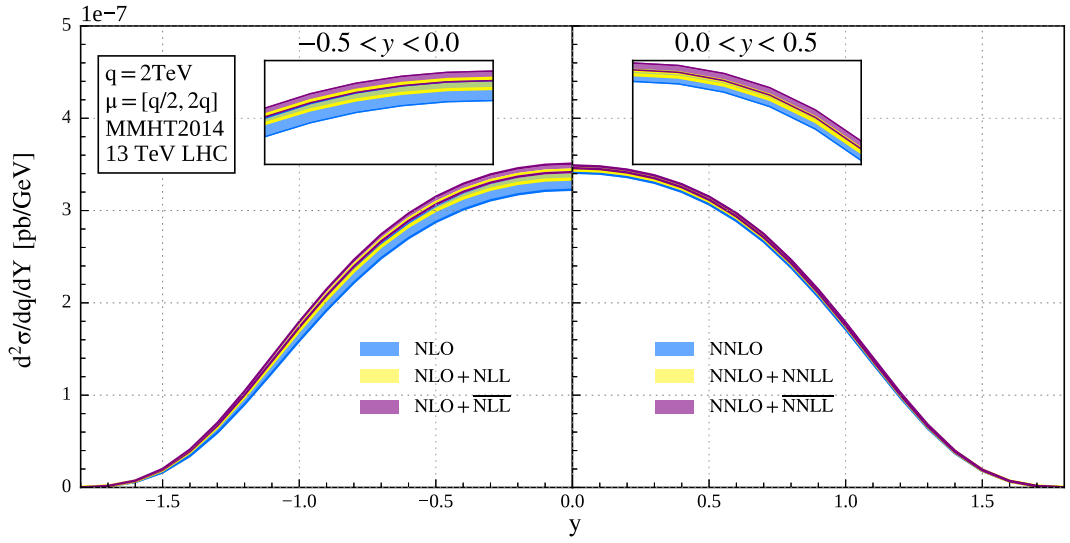

FIG. 7. Comparison of seven-point scale variation between SV and SV + NSV resummed results matched to NLO (left panel) and NNLO (right panel) for $q = 2$ TeV.

TABLE VII. Fixed-order, SV, and SV + NSV resummed cross sections in 10^{-7} pb/GeV with seven-point scale uncertainties in percent around the central scale $\mu_R = \mu_F = 2$ TeV.

y	NLO	NLO + NLL	NLO + $\overline{\text{NLL}}$	NNLO	NNLO + NNLL	NNLO + $\overline{\text{NNLL}}$
0	$3.323^{+2.836\%}_{-2.928\%}$	$3.3927^{+1.380\%}_{-1.5263\%}$	$3.460^{+1.395\%}_{-1.253\%}$	$3.4405^{+0.597\%}_{-0.889\%}$	$3.4503^{+0.226\%}_{-0.337\%}$	$3.470^{+0.533\%}_{-0.312\%}$
0.4	$3.105^{+2.881\%}_{-2.998\%}$	$3.1803^{+1.390\%}_{-1.431\%}$	$3.244^{+1.408\%}_{-1.268\%}$	$3.2328^{+0.600\%}_{-0.919\%}$	$3.2462^{+0.204\%}_{-0.329\%}$	$3.2660^{+0.596\%}_{-0.397\%}$
0.8	$2.295^{+3.079\%}_{-3.290\%}$	$2.3755^{+1.427\%}_{-1.281\%}$	$2.426^{+1.563\%}_{-1.322\%}$	$2.4096^{+0.647\%}_{-1.033\%}$	$2.4298^{+0.308\%}_{-0.276\%}$	$2.446^{+0.790\%}_{-0.653\%}$
1.2	$0.9384^{+3.655\%}_{-3.914\%}$	$0.9946^{+1.528\%}_{-1.399\%}$	$1.0192^{+2.368\%}_{-1.458\%}$	$0.9865^{+0.788\%}_{-1.266\%}$	$1.0044^{+0.725\%}_{-0.583\%}$	$1.0131^{+1.380\%}_{-1.206\%}$

addition of NNLL SV resummed corrections, it gets worse when we include the NSV corrections through $\overline{\text{NNLL}}$. These observations can be seen from the insets in Fig. 8 for lower rapidity values $|y| \leq 0.5$. As we know, the SV resummed terms come only from the diagonal $q\bar{q}$ channel; therefore, they do not need any compensating factor to reduce its uncertainty. In contrary to this, the NSV resummed predictions which we have included here are

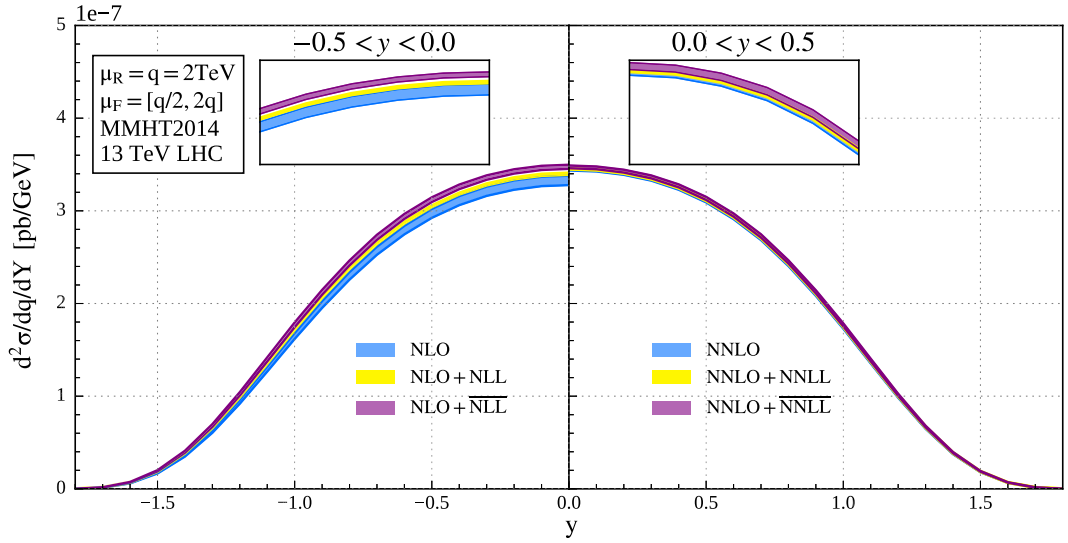

FIG. 8. Comparison of μ_F scale variation between SV and SV + NSV resummed results matched to NLO (left panel) and NNLO (right panel) with the scale μ_R held fixed at $q = 2$ TeV.

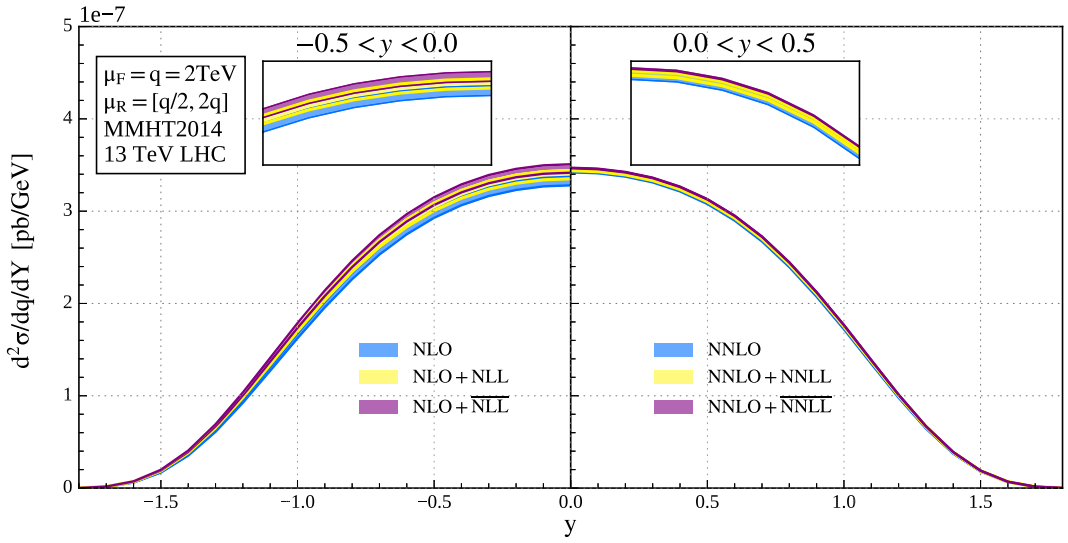

FIG. 9. Comparison of μ_R scale variation between SV and SV + NSV resummed results matched to NLO (left panel) and NNLO (right panel) with the scale μ_F held fixed at $q = 2$ TeV.

incomplete due to missing contributions from the off-diagonal qg channel. Consequently, the NSV included results will show the residual μ_F uncertainty due to mixing of various partonic channels. However, the scenario will be different if we keep the scale μ_F fixed and vary the renormalization scale μ_R.

Figure 9 shows the comparison of SV and SV + NSV resummed results under the μ_R scale variation for $q = 2$ TeV. Here, for the case of μ_R variation as well, the uncertainties of fixed-order results get improved by the inclusion of both SV and NSV resummed corrections. Interestingly, at NNLO, the width of the bands gets reduced substantially when the NSV resummed correction at $\overline{\text{NNLL}}$ accuracy is added in comparison to its SV counterpart. This improvement by the inclusion of $\overline{\text{NNLL}}$ NSV resummed corrections is notable for lower rapidity values $|y| \leq 0.5$ as shown in the insets in Fig. 9. The uncertainty at NNLO around the central rapidity region lies between $(-0.57\%, +0.5\%)$, which gets reduced to $(-0.33\%, +0.22\%)$ when the SV (NNLL) corrections are added. And, it gets further improved to $(-0.16\%, 0\%)$ with the inclusion of NSV corrections ($\overline{\text{NNLL}}$). This emphasizes that the resummed NSV contributions play a vital role in bringing down the μ_R scale uncertainty as we go to higher logarithmic corrections.

In summary, we found that the uncertainty becomes better with the inclusion of both SV (NLL) and NSV ($\overline{\text{NLL}}$) resummed corrections at NLO under μ_F as well as μ_R scale variations. But at NNLO, under μ_F scale variation, the inclusion of NSV $\overline{\text{NNLL}}$ corrections increases the uncertainty, whereas the SV NNLL corrections bring it down significantly. This indicates that the NSV resummed corrections here require the resummed contributions from qg channel as a compensating factor to improve the uncertainty. Note that in all these analyses we studied the impact of fixed order and resummed CFs using same PDF sets to desired logarithmic accuracy for both of them. For studies related to μ_F variations, it is worthwhile to consider resummed PDFs if they are available. However, as far as the μ_R uncertainty is concerned, the NSV corrections show nice behavior especially at NNLO + $\overline{\text{NNLL}}$ accuracy with notable reduction in the uncertainty. This suggests that the resummed NSV terms play a substantial role in improving the μ_R scale uncertainty in comparison to its SV counterpart.

IV. DISCUSSION AND CONCLUSION

Through this article, we provide for the first time the numerical predictions for resummed next-to-soft-virtual contributions up to NNLO + $\overline{\text{NNLL}}$ accuracy to the rapidity distribution of pair of leptons in the Drell-Yan process at the LHC. By restricting ourselves to the mechanism where only neutral gauge bosons like photons and Z bosons produce leptons, we have used our recent formalism [70] to systematically resum NSV logarithms to all orders. In our previous work on the Drell-Yan inclusive cross section, we quantified the significant contribution of the NSV logarithms in the fixed-order predictions [69]. This serves as the motivating factor to study the numerical significance of these collinear logarithms in the case of rapidity distribution as well.

We have quantified the numerical effects of SV + NSV higher-order predictions by providing the K-factor values for central scale $\mu_R = \mu_F = M_Z$. We find that there is an enhancement of 4.9%, 3.98%, and 1.24% at LO + $\overline{\text{LL}}$, NLO + $\overline{\text{NLL}}$, and NNLO + $\overline{\text{NNLL}}$, respectively, by the inclusion of SV + NSV resumed results. Also, there is an improvement in the perturbative convergence over the fixed-order results till NNLO + $\overline{\text{NNLL}}$ accuracy. The sensitivity of our predictions to the unphysical scales μ_R and μ_F is studied using the canonical seven-point scale variation approach. We have given the plot of seven-point scale variation for two values of invariant mass, $q = M_Z$ and $q = 2$ TeV. We find that at $q = M_Z$ the uncertainty of resummed predictions is more than the corresponding fixed-order results till NNLO. However, at $q = 2$ TeV, the scale sensitivity at NLO + $\overline{\text{NLL}}$ is decreased over the entire rapidity region, whereas at NNLO + $\overline{\text{NNLL}}$, it gets reduced around the central rapidity region. Thus, by doing a comparative study of the scale uncertainties at two different q values, we infer that the resummation effects become prominent as we go to higher values of q. Nevertheless, there is a systematic reduction in the uncertainty of the resummed results while moving to higher logarithmic accuracy for both $q = M_z$ and $q = 2$ TeV.

Further analysis of the scale dependency revealed that the seven-point scale uncertainties of resummed predictions are largely governed by the factorization scale μ_F especially at NNLO + $\overline{\text{NNLL}}$. Moreover, the comparative study of SV and SV + NSV resummed results shows that the NSV part of the resummation increases the uncertainty due to μ_F scale variations. We know that different partonic channels mix under factorization scale variations when they are convoluted with appropriate PDFs. Therefore, the absence of NSV contributions coming from the off-diagonal qg channel increases the sensitivity to μ_F scale at the hadronic level. However, this missing compensation from the qg channel is more evident at NNLO level due to considerable contribution from qg channel at this order. This suggests that the NSV resummation corresponding to qg channel is necessary to improve the predictions as we go to higher orders in perturbaton theory. In addition, as far as the μ_F scale variation is concerned, resummed PDFs are also useful to include for better results.

The independent study of renormalization scale variation shows that the improvement in the scale uncertainty at NLO + $\overline{\text{NLL}}$ is not quantitatively significant; however, at NNLO + $\overline{\text{NNLL}}$, there is a substantial decrease in μ_R scale sensitivity as compared to the corresponding fixed-order results. Note that the μ_R scale uncertainty at NNLO is reduced from (−0.56%, +0.5%) to (−0.16%, 0%) for the

central rapidity region by the inclusion of $\overline{\text{NNLL}}$. From the comparison of SV and SV + NSV resummed results, we find that it is the inclusion of NSV resummed corrections at $\overline{\text{NNLL}}$ accuracy to its SV counterpart, which brings down the μ_R scale dependency to a great extent. This is expected because different channels, being renormalization group invariant, do not mix under μ_R scale variation.

ACKNOWLEDGMENTS

We thank J. Michel and F. Tackmann for third-order DY results of rapidity for comparing purposes and C. Duhr and B. Mistlberger for providing third-order results for the inclusive reactions. A. A. H. is supported by the French ANR under Grant No. ANR-20-CE31-0015 (PrecisOnium). In addition, we would also like to thank the computer administrative unit of IMSc for its help and support.

APPENDIX A: NSV RESUMMATION EXPONENTS $\bar{g}^q_{d,i}(\omega)$

The NSV resummation exponents $\bar{g}^q_{d,i}(\omega)$ given in (10) are provided below:

$$\bar{g}^q_{d,1}(\omega) = \frac{1}{\beta_0} C_F \{2L_\omega\}, \tag{A1}$$

$$\bar{g}^q_{d,2}(\omega) = \frac{1}{1-\omega}\left[\frac{1}{\beta_0^2} C_F C_A n_f \left\{-\frac{20}{3}\omega - \frac{20}{3}L_\omega\right\} + \frac{1}{\beta_0^2} C_F C_A^2 \left\{\frac{68}{3}\omega + \frac{68}{3}L_\omega\right\} + \frac{1}{\beta_0^2} C_F^2 n_f \{-4\omega - 4L_\omega\} \right.$$
$$\left. + \frac{1}{\beta_0} C_F n_f \left\{\frac{20}{9}\omega\right\} + \frac{1}{\beta_0} C_F C_A \left\{-\frac{134}{9}\omega + 4\omega\zeta_2\right\} + C_F\{-2 + 2L_{qr} - 2L_{fr} + 2L_{fr}\omega - 4\gamma_E\}\right], \tag{A2}$$

$$\bar{g}^q_{d,3}(\omega) = \frac{1}{(1-\omega)^2}\left[\frac{1}{\beta_0^3} C_F C_A^2 n_f^2 \left\{\frac{100}{9}\omega^2 - \frac{100}{9}L_\omega^2\right\} + \frac{1}{\beta_0^3} C_F C_A^3 n_f \left\{-\frac{680}{9}\omega^2 + \frac{680}{9}L_\omega^2\right\}\right.$$
$$+ \frac{1}{\beta_0^3} C_F C_A^4 \left\{\frac{1156}{9}\omega^2 - \frac{1156}{9}L_\omega^2\right\} + \frac{1}{\beta_0^3} C_F^2 C_A n_f^2 \left\{\frac{40}{3}\omega^2 - \frac{40}{3}L_\omega^2\right\} + \frac{1}{\beta_0^3} C_F^2 C_A^2 n_f \left\{-\frac{136}{3}\omega^2 + \frac{136}{3}L_\omega^2\right\}$$
$$+ \frac{1}{\beta_0^3} C_F^3 n_f^2 \{4\omega^2 - 4L_\omega^2\} + \frac{1}{\beta_0^2} C_F C_A n_f^2 \left\{\frac{200}{27}\omega - \frac{31}{6}\omega^2 + \frac{200}{27}L_\omega\right\}$$
$$+ \frac{1}{\beta_0^2} C_F C_A^2 n_f \left\{-\frac{2020}{27}\omega + \frac{40}{3}\omega\zeta_2 + \frac{1145}{18}\omega^2 - \frac{20}{3}\omega^2\zeta_2 - \frac{2020}{27}L_\omega + \frac{40}{3}L_\omega\zeta_2\right\}$$
$$+ \frac{1}{\beta_0^2} C_F C_A^3 \left\{\frac{4556}{27}\omega - \frac{136}{3}\omega\zeta_2 - \frac{2471}{18}\omega^2 + \frac{68}{3}\omega^2\zeta_2 + \frac{4556}{27}L_\omega - \frac{136}{3}L_\omega\zeta_2\right\}$$
$$+ \frac{1}{\beta_0^2} C_F^2 n_f^2 \left\{\frac{40}{9}\omega - \frac{31}{9}\omega^2 + \frac{40}{9}L_\omega\right\} + \frac{1}{\beta_0^2} C_F^2 C_A n_f \left\{-\frac{268}{9}\omega + 8\omega\zeta_2 + \frac{473}{18}\omega^2 - 4\omega^2\zeta_2 - \frac{268}{9}L_\omega + 8L_\omega\zeta_2\right\}$$
$$+ \frac{1}{\beta_0^2} C_F^3 n_f \{-\omega^2\} + \frac{1}{\beta_0} C_F n_f^2 \left\{\frac{8}{27}\omega - \frac{4}{27}\omega^2\right\} + \frac{1}{\beta_0} C_F C_A n_f \left\{\frac{418}{27}\omega + \frac{56}{3}\omega\zeta_3 - \frac{80}{9}\omega\zeta_2 - \frac{209}{27}\omega^2\right.$$
$$\left. - \frac{28}{3}\omega^2\zeta_3 + \frac{40}{9}\omega^2\zeta_2 - \frac{20}{3}L_\omega + \frac{20}{3}L_\omega L_{qr} - \frac{40}{3}L_\omega\gamma_E\right\} + \frac{1}{\beta_0} C_F C_A^2 \left\{-\frac{245}{3}\omega - \frac{44}{3}\omega\zeta_3 + \frac{536}{9}\omega\zeta_2\right.$$
$$\left. - \frac{88}{5}\omega\zeta_2^2 + \frac{245}{6}\omega^2 + \frac{22}{3}\omega^2\zeta_3 - \frac{268}{9}\omega^2\zeta_2 + \frac{44}{5}\omega^2\zeta_2^2 + \frac{68}{3}L_\omega - \frac{68}{3}L_\omega L_{qr} + \frac{136}{3}L_\omega\gamma_E\right\}$$
$$+ \frac{1}{\beta_0} C_F^2 n_f \left\{\frac{55}{3}\omega - 16\omega\zeta_3 - \frac{55}{6}\omega^2 + 8\omega^2\zeta_3 - 4L_\omega + 4L_\omega L_{qr} - 8L_\omega\gamma_E\right\} + C_F n_f \left\{\frac{116}{27} - \frac{32}{9}L_{qr} + \frac{2}{3}L_{qr}^2\right.$$
$$\left. + \frac{20}{9}L_{fr} - \frac{40}{9}L_{fr}\omega + \frac{20}{9}L_{fr}\omega^2 - \frac{2}{3}L_{fr}^2 + \frac{4}{3}L_{fr}^2\omega - \frac{2}{3}L_{fr}^2\omega^2 + \frac{64}{9}\gamma_E - \frac{8}{3}\gamma_E L_{qr} + \frac{8}{3}\gamma_E^2\right\}$$
$$+ C_F C_A \left\{-\frac{806}{27} + 14\zeta_3 + 4\zeta_2 + \frac{200}{9}L_{qr} - 4L_{qr}\zeta_2 - \frac{11}{3}L_{qr}^2 - \frac{134}{9}L_{fr} + 4L_{fr}\zeta_2 + \frac{268}{9}L_{fr}\omega - 8L_{fr}\omega\zeta_2\right.$$
$$\left.\left. - \frac{134}{9}L_{fr}\omega^2 + 4L_{fr}\omega^2\zeta_2 + \frac{11}{3}L_{fr}^2 - \frac{22}{3}L_{fr}^2\omega + \frac{11}{3}L_{fr}^2\omega^2 - \frac{400}{9}\gamma_E + 8\gamma_E\zeta_2 + \frac{44}{3}\gamma_E L_{qr} - \frac{44}{3}\gamma_E^2\right\}\right]. \tag{A3}$$

APPENDIX B: NSV RESUMMATION EXPONENTS $h^q_{d,ij}(\omega)$

The NSV resummation exponents $h^q_{d,ij}(\omega)$ given in (11) are provided below:

$$h^q_{d,00}(\omega) = \frac{1}{\beta_0} C_F\{-4L_\omega\}, \qquad h^q_{d,01}(\omega) = 0, \tag{B1}$$

$$\begin{aligned} h^q_{d,10}(\omega) = \frac{1}{2\beta_0^2(\omega-1)} \Bigg[& \beta_1 C_F\{8\omega + 8L_\omega\} + \beta_0 C_F n_f \left\{\frac{80}{9}\omega\right\} + \beta_0 C_F C_A \left\{-\frac{536}{9}\omega + 16\omega\zeta_2\right\} \\ & + \beta_0 C_F^2\{24\omega - 32\gamma_E\omega\} + \beta_0^2 C_F\{-4 - 8\omega - 8L_{fr} + 8L_{fr}\omega + 8L_{qr} - 16\gamma_E\}\Bigg], \end{aligned} \tag{B2}$$

$$h^q_{d,11}(\omega) = \frac{C_F^2}{2\beta_0(\omega-1)^2}\{28\omega - 32\omega^2\}, \tag{B3}$$

$$\begin{aligned} h^q_{d,20}(\omega) = \frac{1}{2\beta_0^3(\omega-1)^2} \Bigg[& \beta_1^2 C_F\{-4\omega^2 + 4L_\omega^2\} + \beta_0\beta_2 C_F\{4\omega^2\} + \beta_0\beta_1 C_F n_f \left\{\frac{80}{9}\omega - \frac{40}{9}\omega^2 + \frac{80}{9}L_\omega\right\} \\ & + \beta_0\beta_1 C_F C_A \left\{-\frac{536}{9}\omega + 16\omega\zeta_2 + \frac{268}{9}\omega^2 - 8\omega^2\zeta_2 - \frac{536}{9}L_\omega + 16L_\omega\zeta_2\right\} \\ & + \beta_0\beta_1 C_F^2\{24\omega - 12\omega^2 - 32\gamma_E\omega + 16\gamma_E\omega^2 + 24L_\omega - 32L_\omega\gamma_E\} + \beta_0^2 C_F n_f^2 \left\{-\frac{32}{27}\omega + \frac{16}{27}\omega^2\right\} \\ & + \beta_0^2 C_F C_A n_f \left\{-\frac{1672}{27}\omega - \frac{224}{3}\omega\zeta_3 + \frac{320}{9}\omega\zeta_2 + \frac{836}{27}\omega^2 + \frac{112}{3}\omega^2\zeta_3 - \frac{160}{9}\omega^2\zeta_2\right\} \\ & + \beta_0^2 C_F C_A^2 \left\{\frac{980}{3}\omega + \frac{176}{3}\omega\zeta_3 - \frac{2144}{9}\omega\zeta_2 + \frac{352}{5}\omega\zeta_2^2 - \frac{490}{3}\omega^2 - \frac{88}{3}\omega^2\zeta_3 + \frac{1072}{9}\omega^2\zeta_2 - \frac{176}{5}\omega^2\zeta_2^2\right\} \\ & + \beta_0^2 C_F^2 n_f \left\{-44\omega + 64\omega\zeta_3 + \frac{64}{3}\omega\zeta_2 + 22\omega^2 - 32\omega^2\zeta_3 - \frac{32}{3}\omega^2\zeta_2 - \frac{640}{9}\gamma_E\omega + \frac{320}{9}\gamma_E\omega^2\right\} \\ & + \beta_0^2 C_F^2 C_A \left\{-\frac{604}{3}\omega + 96\omega\zeta_3 - \frac{208}{3}\omega\zeta_2 + \frac{302}{3}\omega^2 - 48\omega^2\zeta_3 + \frac{104}{3}\omega^2\zeta_2 + \frac{4288}{9}\gamma_E\omega - 128\gamma_E\omega\zeta_2\right. \\ & \left. - \frac{2144}{9}\gamma_E\omega^2 + 64\gamma_E\omega^2\zeta_2\right\} + \beta_0^2 C_F^3\{-12\omega - 192\omega\zeta_3 + 96\omega\zeta_2 + 6\omega^2 + 96\omega^2\zeta_3 - 48\omega^2\zeta_2\} \\ & + \beta_0^2\beta_1 C_F\{-12L_\omega + 8L_\omega L_{qr} - 16L_\omega\gamma_E\} + \beta_0^3 C_F n_f \left\{-\frac{536}{27} + \frac{32}{3}\zeta_2 - \frac{80}{9}\omega + \frac{40}{9}\omega^2 - \frac{80}{9}L_{fr}\right. \\ & \left. + \frac{160}{9}L_{fr}\omega - \frac{80}{9}L_{fr}\omega^2 + \frac{80}{9}L_{qr} - \frac{160}{9}\gamma_E\right\} + \beta_0^3 C_F C_A \left\{\frac{2000}{27} - 56\zeta_3 - \frac{200}{3}\zeta_2 + \frac{536}{9}\omega - 16\omega\zeta_2\right. \\ & \left. - \frac{268}{9}\omega^2 + 8\omega^2\zeta_2 + \frac{536}{9}L_{fr} - 16L_{fr}\zeta_2 - \frac{1072}{9}L_{fr}\omega + 32L_{fr}\omega\zeta_2 + \frac{536}{9}L_{fr}\omega^2 - 16L_{fr}\omega^2\zeta_2 - \frac{536}{9}L_{qr}\right. \\ & \left. + 16L_{qr}\zeta_2 + \frac{892}{9}\gamma_E - 32\gamma_E\zeta_2\right\} + \beta_0^3 C_F^2\{-8\zeta_2 - 24L_{fr} + 48L_{fr}\omega - 24L_{fr}\omega^2 + 24L_{qr} - 28\gamma_E \\ & + 32\gamma_E L_{fr} - 64\gamma_E L_{fr}\omega + 32\gamma_E L_{fr}\omega^2 - 32\gamma_E L_{qr} + 56\gamma_E^2\} + \beta_0^4 C_F\{16\zeta_2 + 8L_{fr} - 16L_{fr}\omega + 8L_{fr}\omega^2 \\ & - 4L_{fr}^2 + 8L_{fr}^2\omega - 4L_{fr}^2\omega^2 - 12L_{qr} + 4L_{qr}^2 + 24\gamma_E - 16\gamma_E L_{qr} + 16\gamma_E^2\}\Bigg], \end{aligned} \tag{B4}$$

$$\begin{aligned} h^q_{d,21}(\omega) = \frac{1}{2\beta_0^2(\omega-1)^2}\beta_1 \Bigg[& C_F^2\{-32\omega + 16\omega^2 - 32L_\omega\} + \beta_0 C_F^2 n_f \left\{-\frac{640}{9}\omega + \frac{320}{9}\omega^2\right\} \\ & + \beta_0 C_F^2 C_A \left\{\frac{4288}{9}\omega - 128\omega\zeta_2 - \frac{2144}{9}\omega^2 + 64\omega^2\zeta_2\right\} + \beta_0^2 C_F C_A\{-20\} \\ & + \beta_0^2 C_F^2\{20 + 32L_{fr} - 64L_{fr}\omega + 32L_{fr}\omega^2 - 32L_{qr} + 48\gamma_E\}\Bigg], \end{aligned} \tag{B5}$$

$$h^q_{d,22}(\omega) = \frac{1}{2\beta_0(\omega-1)^3}\left[C_F^2 n_f\left\{\frac{32}{27}\omega\right\} + C_F^2 C_A\left\{-\frac{176}{27}\omega\right\}\right], \tag{B6}$$

where γ_E is the Euler-Mascheroni constant. Here, $L_\omega = \ln(1-\omega)$ with $\omega = \beta_0 a_s(\mu_R^2)\ln N_1 N_2$, $L_{qr} = \ln(\frac{q^2}{\mu_R^2})$ and $L_{fr} = \ln(\frac{\mu_F^2}{\mu_R^2})$.

[1] S. Drell and T.-M. Yan, Phys. Rev. Lett. **25**, 316 (1970); **25**, 902(E) (1970).
[2] V. A. Khoze, A. D. Martin, R. Orava, and M. G. Ryskin, Eur. Phys. J. C **19**, 313 (2001).
[3] A. Accardi *et al.*, Eur. Phys. J. C **76**, 471 (2016).
[4] I. Scimemi and A. Vladimirov, Eur. Phys. J. C **78**, 89 (2018).
[5] I. Scimemi and A. Vladimirov, J. High Energy Phys. 08 (2018) 003.
[6] G. Altarelli, R. Ellis, and G. Martinelli, Nucl. Phys. **B143**, 521 (1978).
[7] G. Altarelli, R. Ellis, and G. Martinelli, Nucl. Phys. **B157**, 461 (1979).
[8] R. Hamberg, W. L. van Neerven, and T. Matsuura, Nucl. Phys. **B359**, 343 (1991); **B644**, 403(E) (2002).
[9] R. V. Harlander and W. B. Kilgore, Phys. Rev. Lett. **88**, 201801 (2002).
[10] T. Ahmed, M. Mahakhud, N. Rana, and V. Ravindran, Phys. Rev. Lett. **113**, 112002 (2014).
[11] Y. Li, A. von Manteuffel, R. M. Schabinger, and H. X. Zhu, Phys. Rev. D **90**, 053006 (2014).
[12] C. Duhr, F. Dulat, and B. Mistlberger, Phys. Rev. Lett. **125**, 172001 (2020).
[13] S. Dittmaier and M. Krämer, Phys. Rev. D **65**, 073007 (2002).
[14] U. Baur, O. Brein, W. Hollik, C. Schappacher, and D. Wackeroth, Phys. Rev. D **65**, 033007 (2002).
[15] R. K. Ellis, G. Martinelli, and R. Petronzio, Nucl. Phys. **B211**, 106 (1983).
[16] C. Anastasiou, L. J. Dixon, K. Melnikov, and F. Petriello, Phys. Rev. Lett. **91**, 182002 (2003).
[17] C. Anastasiou, L. J. Dixon, K. Melnikov, and F. Petriello, Phys. Rev. D **69**, 094008 (2004).
[18] S. Catani, L. Cieri, G. Ferrera, D. de Florian, and M. Grazzini, Phys. Rev. Lett. **103**, 082001 (2009).
[19] K. Melnikov and F. Petriello, Phys. Rev. D **74**, 114017 (2006).
[20] V. Ravindran, J. Smith, and W. L. van Neerven, Nucl. Phys. **B767**, 100 (2007).
[21] V. Ravindran and J. Smith, Phys. Rev. D **76**, 114004 (2007).
[22] R. Gavin, Y. Li, F. Petriello, and S. Quackenbush, Comput. Phys. Commun. **184**, 208 (2013).
[23] T. Ahmed, M. K. Mandal, N. Rana, and V. Ravindran, Phys. Rev. Lett. **113**, 212003 (2014).
[24] X. Chen, T. Gehrmann, N. Glover, A. Huss, T.-Z. Yang, and H. X. Zhu, Phys. Rev. Lett. **128**, 052001 (2022).
[25] Y. Li and F. Petriello, Phys. Rev. D **86**, 094034 (2012).
[26] S. Frixione and B. R. Webber, J. High Energy Phys. 06 (2002) 029.
[27] S. Frixione, P. Nason, and C. Oleari, J. High Energy Phys. 11 (2007) 070.
[28] J. Alwall, R. Frederix, S. Frixione, V. Hirschi, F. Maltoni, O. Mattelaer, H. S. Shao, T. Stelzer, P. Torrielli, and M. Zaro, J. High Energy Phys. 07 (2014) 079.
[29] G. F. Sterman, Nucl. Phys. **B281**, 310 (1987).
[30] S. Catani and L. Trentadue, Nucl. Phys. **B327**, 323 (1989).
[31] S. Catani and L. Trentadue, Nucl. Phys. **B353**, 183 (1991).
[32] S. Moch and A. Vogt, Phys. Lett. B **631**, 48 (2005).
[33] E. Laenen and L. Magnea, Phys. Lett. B **632**, 270 (2006).
[34] A. Idilbi, X.-d. Ji, J.-P. Ma, and F. Yuan, Phys. Rev. D **73**, 077501 (2006).
[35] V. Ravindran, Nucl. Phys. **B746**, 58 (2006).
[36] J. C. Collins, D. E. Soper, and G. F. Sterman, Nucl. Phys. **B250**, 199 (1985).
[37] S. Catani, D. de Florian, and M. Grazzini, Nucl. Phys. **B596**, 299 (2001).
[38] A. Idilbi and X.-d. Ji, Phys. Rev. D **72**, 054016 (2005).
[39] T. Becher and M. Neubert, Eur. Phys. J. C **71**, 1665 (2011).
[40] D. Westmark and J. F. Owens, Phys. Rev. D **95**, 056024 (2017).
[41] A. Mukherjee and W. Vogelsang, Phys. Rev. D **73**, 074005 (2006).
[42] E. Laenen and G. F. Sterman, in *Proceedings of the 7th Meeting of the APS Division of Particles Fields* (World Scientific, Singapore, 1993), pp. 987–989.
[43] P. Bolzoni, Phys. Lett. B **643**, 325 (2006).
[44] M. Bonvini, S. Forte, and G. Ridolfi, Nucl. Phys. **B847**, 93 (2011).
[45] T. Becher and M. Neubert, Phys. Rev. Lett. **97**, 082001 (2006).
[46] T. Becher, M. Neubert, and G. Xu, J. High Energy Phys. 07 (2008) 030.
[47] P. Banerjee, G. Das, P. K. Dhani, and V. Ravindran, Phys. Rev. D **97**, 054024 (2018).
[48] P. Banerjee, G. Das, P. K. Dhani, and V. Ravindran, Phys. Rev. D **98**, 054018 (2018).
[49] T. Ahmed, M. K. Mandal, N. Rana, and V. Ravindran, J. High Energy Phys. 02 (**2015**) 131.
[50] C. Anastasiou, C. Duhr, F. Dulat, F. Herzog, and B. Mistlberger, Phys. Rev. Lett. **114**, 212001 (2015).
[51] C. Duhr, F. Dulat, and B. Mistlberger, Phys. Rev. Lett. **125**, 051804 (2020).

[52] F. Dulat, B. Mistlberger, and A. Pelloni, Phys. Rev. D **99**, 034004 (2019).
[53] E. Laenen, L. Magnea, and G. Stavenga, Phys. Lett. B **669**, 173 (2008).
[54] E. Laenen, L. Magnea, G. Stavenga, and C. D. White, J. High Energy Phys. 01 (**2011**) 141.
[55] D. Bonocore, E. Laenen, L. Magnea, L. Vernazza, and C. D. White, Phys. Lett. B **742**, 375 (2015).
[56] D. Bonocore, E. Laenen, L. Magnea, S. Melville, L. Vernazza, and C. White, J. High Energy Phys. 06 (2015) 008.
[57] D. Bonocore, E. Laenen, L. Magnea, L. Vernazza, and C. White, J. High Energy Phys. 12 (2016) 121.
[58] V. Del Duca, E. Laenen, L. Magnea, L. Vernazza, and C. White, J. High Energy Phys. 11 (2017) 057.
[59] N. Bahjat-Abbas, D. Bonocore, J. Sinninghe Damsté, E. Laenen, L. Magnea, L. Vernazza, and C. White, J. High Energy Phys. 11 (2019) 002.
[60] G. Soar, S. Moch, J. Vermaseren, and A. Vogt, Nucl. Phys. **B832**, 152 (2010).
[61] S. Moch and A. Vogt, J. High Energy Phys. 11 (2009) 099.
[62] D. de Florian, J. Mazzitelli, S. Moch, and A. Vogt, J. High Energy Phys. 10 (2014) 176.
[63] M. Beneke, A. Broggio, M. Garny, S. Jaskiewicz, R. Szafron, L. Vernazza, and J. Wang, J. High Energy Phys. 03 (2019) 043.
[64] M. Beneke, M. Garny, S. Jaskiewicz, R. Szafron, L. Vernazza, and J. Wang, J. High Energy Phys. 01 (2020) 094.
[65] M. Beneke, A. Broggio, S. Jaskiewicz, and L. Vernazza, J. High Energy Phys. 07 (**2020**) 078.
[66] A. Ajjath, P. Mukherjee, and V. Ravindran, Phys. Rev. D **105**, 094035 (2022).
[67] A. Ajjath, P. Mukherjee, V. Ravindran, A. Sankar, and S. Tiwari, J. High Energy Phys. 04 (2021) 131.
[68] A. H. Ajjath, P. Mukherjee, V. Ravindran, A. Sankar, and S. Tiwari, arXiv:2109.12657.
[69] A. H. Ajjath, P. Mukherjee, V. Ravindran, A. Sankar, and S. Tiwari, Eur. Phys. J. C **82**, 234 (2022).
[70] A. H. Ajjath, P. Mukherjee, V. Ravindran, A. Sankar, and S. Tiwari, Phys. Rev. D **103**, L111502 (2021).
[71] T. Ahmed, A. A. H., P. Mukherjee, V. Ravindran, and A. Sankar, Eur. Phys. J. C **81**, 943 (2021).
[72] S. Moch, J. A. M. Vermaseren, and A. Vogt, Nucl. Phys. **B688**, 101 (2004).
[73] A. Vogt, S. Moch, and J. A. M. Vermaseren, Nucl. Phys. **B691**, 129 (2004).
[74] J. Blümlein, P. Marquard, C. Schneider, and K. Schönwald, Nucl. Phys. **B971**, 115542 (2021).
[75] P. Banerjee, P. K. Dhani, M. C. Kumar, P. Mathews, and V. Ravindran, Phys. Rev. D **97**, 094028 (2018).
[76] T. Ahmed, A. A. H., P. Mukherjee, V. Ravindran, and A. Sankar, Eur. Phys. J. C **81**, 943 (2021).
[77] L. A. Harland-Lang, A. D. Martin, P. Motylinski, and R. S. Thorne, Eur. Phys. J. C **75**, 204 (2015).
[78] A. Buckley, J. Ferrando, S. Lloyd, K. Nordstrm, B. Page, M. Rfenacht, M. Schnherr, and G. Watt, Eur. Phys. J. C **75**, 132 (2015).
[79] P. A. Zyla *et al.* (Particle Data Group), Prog. Theor. Exp. Phys. **2020**, 083C01 (2020).
[80] A. Vogt, Comput. Phys. Commun. **170**, 65 (2005).
[81] S. Catani, D. de Florian, M. Grazzini, and P. Nason, J. High Energy Phys. 07 (2003) 028.
[82] S. Catani, M. L. Mangano, P. Nason, and L. Trentadue, Nucl. Phys. **B478**, 273 (1996).
[83] G. Lustermans, J. K. L. Michel, and F. J. Tackmann, arXiv:1908.00985.
[84] C. Anastasiou, C. Duhr, F. Dulat, E. Furlan, T. Gehrmann, F. Herzog, and B. Mistlberger, J. High Energy Phys. 03 (2015) 091.